



Aqueous Multivalent Charge Storage Mechanism in Aromatic Diamine-Based Organic Electrodes

Selin Sariyer, Arpita Ghosh, Sevde Nazli Dambasan, El Mahdi Halim, Mama El Rhazi, Hubert Perrot, Ozlem Sel, Rezan Demir-Cakan

► To cite this version:

Selin Sariyer, Arpita Ghosh, Sevde Nazli Dambasan, El Mahdi Halim, Mama El Rhazi, et al.. Aqueous Multivalent Charge Storage Mechanism in Aromatic Diamine-Based Organic Electrodes. ACS Applied Materials & Interfaces, 2022, 14 (6), pp.8508-8520. 10.1021/acsami.1c19607 . hal-03611967

HAL Id: hal-03611967

<https://hal.science/hal-03611967>

Submitted on 14 Nov 2022

HAL is a multi-disciplinary open access archive for the deposit and dissemination of scientific research documents, whether they are published or not. The documents may come from teaching and research institutions in France or abroad, or from public or private research centers.

L'archive ouverte pluridisciplinaire **HAL**, est destinée au dépôt et à la diffusion de documents scientifiques de niveau recherche, publiés ou non, émanant des établissements d'enseignement et de recherche français ou étrangers, des laboratoires publics ou privés.

Aqueous Multivalent Charge Storage Mechanism in Aromatic Diamine Based Organic Electrodes

Selin Sariyer^a, Arpita Ghosh^b, Sevde Nazli Dambasan^a, El Mahdi Halim^{b,c}, Mama El Rhazfi, Hubert

Perrot^b, Ozlem Sel^{b,*} and Rezan Demir-Cakan^{a,*}

^a Gebze Technical University, Department of Chemical Engineering, 41400 Gebze, Kocaeli, Turkey

^b Sorbonne Université, CNRS, Laboratoire Interfaces et Systèmes Electrochimiques, LISE, 75005 Paris, France

^c University of Hassan II of Casablanca, Faculty of Sciences and Technology, Laboratory of Materials, Membranes and Environment -BP 146, 20650 Mohammedia, Morocco

Abstract

Rechargeable batteries employing aqueous electrolytes are more reliable and cost effective as well as possess high ionic conductivity compared to the flammable organic electrolyte solutions. Among these type of batteries, aqueous batteries with multivalent ions attract more attention in terms of providing high energy density. Herein, electrochemical behavior of an organic electrode based on highly aromatic polymer containing 2,3-diaminophenazine repeating unit, namely poly(ortho-phenylenediamine) (PoPD), is tested in two different multivalent ions (Zn^{2+} and Al^{3+}) containing aqueous electrolytes, *i.e.*, in zinc sulfate and aluminum chloride solutions. PoPD is synthesized *via* electro-polymerization and its ion transport and storage mechanism are comprehensively investigated by structural and electrochemical analyses. The electrochemical quartz crystal microbalance (EQCM), time-dependent FTIR and EIS analyses as well as ex-situ XRD observations established that along with the Zn^{2+} or Al^{3+} ions, reversible proton insertion/extraction also takes place. Contrary to the most of the organic electrodes that requires the use of conductive carbon additives, electrodeposited PoPD electrode is intrinsically electrically conductive enough, resulting in a carbon-free electrode assembly. In addition, its discharge products do not dissolve in aqueous medium. As a whole, the resulting PoPD electrode delivers excellent rate performances with prolonged cycle life in which discharge capacity of $\sim 110 \text{ mAh g}^{-1}$ in 0.25 M AlCl_3 and

~93 mAh g⁻¹ in 1 M ZnSO₄ aqueous electrolyte after 1000 cycles at a current density of 5C have been achieved.

Keywords: aqueous electrolyte batteries, multivalent ions, organic electrodes, EQCM, electrode/electrolyte interface

1. Introduction

The 2000 Nobel Prize (Heeger, MacDiarmid and Shirakawa) in conductive polymers (CPs) persuades the academic and industrial community to turn their attention towards CPs owing to a vast domain of implementations ranging from electrochemical energy storage to bioelectronics or bio(chemical)sensors.¹⁻

² Considering the increasing energy consumption and the demand for the clean resources, rechargeable batteries are regarded as one of the most appealing alternatives.³ Especially, aqueous rechargeable metal-ion batteries as electrochemical energy storage devices are promising due to their safety, low manufacturing cost, environmental benignity, nontoxicity and high ionic conductivity.⁴ Moreover, multivalent-ion aqueous batteries including Al³⁺, Ca²⁺, Mg²⁺ or Zn²⁺ provide much higher volumetric energy density compared to the monovalent-ion counterparts.⁵

Among multivalent-ion aqueous rechargeable systems, zinc-ion battery (ZIBs) and aluminum-ion battery (AIBs) attract tremendous interest due to high theoretical volumetric capacities of aluminum (8034 mAh cm⁻³) and zinc (5857 mAh cm⁻³) originating from the multi-electron transfer during electrochemical process.⁶⁻⁸ Moreover, aluminum is the third most abundant element in the Earth's crust, facilitating a more affordable manufacturing cost. On the other hand, from the active material utilization point of view, zinc possesses high theoretical capacity of 820 mAh g⁻¹ compared to other metal-ion batteries and high compatibility with aqueous electrolyte, which make zinc a promising anode material for ZIBs.⁴ However, passivation layer on aluminum anode, hydrogen evolution and corrosion restrict the utilization of aluminum

metal in aqueous environment.⁹ In order to overcome these problems, aluminum anode is preferred to be used with the combination of imidazolium salts and aluminum chloride (ionic liquid (IL)) electrolyte.¹⁰

Among the class of organic electrode choices,¹¹⁻¹² CPs such as polyaniline (PANI),¹³ polypyrrole (PPy),¹⁴ polythiophene (PTh), poly-(*p*-phenylene) (PPP) and poly(3,4-ethylenedioxythiophene) (PEDOT)¹⁵ have commonly been used as electroactive materials in ZIBs as well as AIBs. Proposed redox mechanism for charge storage is based on the abundance of delocalized π electrons in CP which facilitate anions/cations insertion during discharge/charge process as well as high local proton storage ability of polymer backbones.¹⁶ Although the electrochemical performance of CPs in ZIBs have been comprehensively investigated,¹² aluminum system is mostly studied in molten salt or in ionic liquids (ILs) containing AlCl_3 and 1-ethyl-3-methylimidazolium (PPy,¹⁷ polythiophene (PTh),¹⁸ PANI,¹⁹ poly-(*p*-phenylene) (PPP)²⁰), only a few studies have shown the electrochemical activity of CPs in rechargeable aluminum-ion batteries in aqueous medium.²¹

Phenylenediamines (-orto, -meta, -para directed) including active amino and imino groups are classified as aromatic diamines.²² Polymerization of phenylenediamine takes place *via* chemical and electrochemical oxidation process,²³ and obtained conductive polymers have been broadly utilized in multiple applications such as sensors,²⁴ supercapacitors,²⁵ anodes for Li-ion batteries in organic electrolytes.²⁶ Electrochemical performance of PoPD has also been evaluated in aqueous metal-ion batteries. *Sivakkumar et al.* synthesized PoPD on carbon electrode and tested in 1 M zinc sulfate (pH= 4) electrolyte in which a discharge capacity of 127 mAh g^{-1} was achieved.²⁷ In a recent study, PoPD was employed as a positive electrode for zinc-ion aqueous battery in which C=N bond of phenazine unit was found to be responsible for zinc ion storage.²⁸

As an extension to previous studies, herein, electrochemical performance of the electropolymerized PoPD electrodes was investigated in two different aqueous electrolytes containing zinc sulfate and aluminum chloride. Our aim is to clarify the nature of the ions (Zn^{2+} , Al^{3+} or other ions included in the electrolyte) taking part in the charge compensation, as well as any other interfacial process that may intervene with

ions' interaction with the electrode material. To the best of our knowledge, this is the first report investigating both the performance and the storage mechanism of a conducting polymer electrode in aqueous Al^{3+} or Zn^{2+} containing electrolyte in a comparative manner. To elucidate the performance and the charge storage properties, cyclic voltammetry (CV), galvanostatic charge-discharge (GCD), electrochemical impedance spectroscopy (EIS) were employed and complemented with time dependent FTIR and *ex-situ* XRD analyses to acquire compositional and structural information. Additionally, to reach a mechanistic understanding of the nature of the ions taking part in the charge storage, we have employed *in situ* Electrochemical Quartz Crystal Microbalance (EQCM) based methods.²⁹⁻³¹ *In-situ* EQCM and EQCM with motional resistance (EQCM-R) or dissipation monitoring (EQCM-D),³²⁻³⁶ have been shown to be beneficial in the gravimetric,^{34, 36} structural,³⁷ and viscoelastic property³⁸ analysis of energy storage materials. To perform such analyses, the PoPD electrodes were electrodeposited as thin layers on the conductive electrode of a quartz crystal resonator and were used as working electrodes. The frequency as well as motional resistance changes (Δf and ΔR_m) occurring in response to an electrochemical process (*e.g.*, insertion of Zn^{2+} or Al^{3+}) at the electrode/electrolyte interface are concurrently monitored and interpreted in correlating with the other (electro)chemical results obtained.

2. Experimental Section

2.1 Preparation of PoPD Electrode: Electro-polymerization of oPD monomer was performed *via* CV, using a three-electrode configuration. In this latter, graphite plate was used as a working electrode ($\sim 2 \text{ cm}^2$), a platinum wire as a counter electrode, and an Ag/AgCl (saturated 3.5 M KCl) was used as a reference electrode. Firstly, 1,2-diaminobenzene (oPD) monomer (Sigma-Aldrich) (5 mM) was dissolved in 0.1 M H_2SO_4 solution and then, followed by electrodeposition on the graphite plate for 1000 polymerization cycles in a potential range from -0.4 V to 0.8 V *vs.* Ag/AgCl (saturated 3.5 M KCl) with a scan rate of 50 mV s^{-1} . Before and after electro-polymerization process, graphite plate was weighed to

determine the active mass of the PoPD electrode. The as synthesized PoPD electrode was used for the electrochemical tests without any further modification.

EQCM (Electrochemical Quartz Crystal Microbalance) measurements were carried out using AT-cut 9 MHz quartz resonators (AWS, Valencia, Spain) modified with gold electrodes as substrates. Electrochemical polymerization of oPD monomer (1,2-diaminobenzene) was carried out according to previously reported literature.³⁹⁻⁴⁰ Briefly, 5 mM oPD was dissolved in 0.1 M H₂SO₄ and cycled 200 times within the potential range of -0.4 V and 0.8 V *vs.* Ag/AgCl at a scan rate of 50 mV s⁻¹. In order to keep the gravimetric regime of the microbalance, the number of cycles have been restricted to 200 (unlike the graphite surface) which gives sufficient coverage of PoPD film on the gold electrode (0.2 cm²) of the quartz resonator.

2.2 Morphological and Compositional Characterization of PoPD Electrode: Functional groups of PoPD were investigated using Fourier-transformed infrared (FTIR) (Perkin Elmer Spectrum 100). Scanning electron microscopy (SEM) (FEI PHILIPS, XL30 SFEG SEM) conjugated with Energy Dispersive X-Ray Spectroscopy (EDS) was employed to examine the surface morphology and elemental analysis of PoPD surface. X-Ray Diffraction patterns of PoPD and graphite were recorded by using X-Ray diffraction Bruker- D8 Advance Bruker AXS.

2.3 Electrochemical Measurements on Zn/PoPD and Al/PoPD Cells: Zn/PoPD cell was fabricated using PoPD electrode as cathode, Pt wire as counter electrode, Ag/AgCl (sat. 3.5 M KCl) as reference electrode and 1 M ZnSO₄ aqueous solution as electrolyte. Al/PoPD cell was tested with the same configuration with 0.25 M AlCl₃ aqueous solution as the electrolyte. The active mass loading of the PoPD electrode is 0.15 mg per cm² on graphite electrodes and it has been kept fixed for both the Zn and Al systems during electrochemical measurements. During the galvanostatic cycling, 1C current density corresponds to 496 mA g⁻¹ in Zn²⁺ containing electrolyte and 744 mA g⁻¹ in Al³⁺ containing electrolyte. The CV (at a scan rate of 1, 5 and 10 mV s⁻¹) and the GCD tests were carried out in a potential range of -0.95 to 0.8 V *vs* Ag/AgCl (sat. 3.5 M KCl) in three-electrode cell configuration for both Zn/PoPD and Al/PoPD

systems. Electrochemical impedance spectroscopy (EIS) was carried out at open circuit voltage (OCV), before and after 1000 cycles at a frequency range of 100 kHz to 1 mHz. All the electrochemical studies were carried out by Bio-Logic VMP3 potentiostat/galvanostat. The ionic conductivity and pH of different concentrations of aqueous electrolytes were measured by HANNA HI2315 conductivity meter and HANNA pH meter (egde HI2002-02), respectively.

EQCM measurements were carried out in 1 M ZnSO₄ and 0.25 M AlCl₃ aqueous solution in a three-electrode configuration using a Bio-Logic electrochemical workstation (Biologic SP200) coupled with a lab-made QCM device. As deposited PoPD films, platinum wire and Ag/AgCl electrode were used as the working, counter and reference electrodes, respectively. The EQCM with motional resistance monitoring were conducted by an Agilent 4294A impedance analyzer coupled with a Bio-Logic electrochemical workstation (Biologic SP200).

The mass variation (Δm) can be derived from the frequency variation (Δf) of the QCM using the Sauerbrey equation⁴¹: ($\Delta f = -k_s \cdot \Delta m$, where, $k_s = 16.31 \times 10^7 \text{ Hz g}^{-1} \text{ cm}^2$, is the experimental sensitivity coefficient). Then, the average mass per electron, $MPE = \frac{n.F.\Delta m}{\Delta Q}$ (n is the number of electrons transferred), can be calculated which estimates the nature of the transferred species (anion, cation, water molecules) during cycling. The negative and positive signs of MPE (mass per electron) correspond to the cationic and anionic contributions, respectively.

3. Results and Discussions

3.1 Electrode preparation and characterization: Electro-polymerization of oPD monomer on graphite plate was performed in acidic environment using cyclic voltammetry. As shown in Figure 1a, during the electrodeposition of PoPD on graphite, intensity of irreversible anodic peak at 0.8 V was decreased gradually due to the decline in activity of monomer, owing to the freshly formed PoPD polymer.⁴² However, the current of the cathodic and anodic peaks (at -0.17 V and -0.10 V, respectively) were increased progressively for the subsequent CV cycles, indicating the growth of PoPD. Electrochemical synthesis of

PoPD was limited to 1000 CV cycles for our study in order to inhibit the non-electroactive polymer films formed for the following cycles. *Malinauskas et al.* concluded that particular thickness of PoPD layer could be obtained *via* anodic electro-polymerization method owing to the low electrical conductivity of PoPD.⁴³ *Yano et al.* reported that the thickness of PoPD film on ITO electrode could not be more than 0.85 μm corresponding 1000 CV cycles.⁴⁴ Consequently, common electro-polymerization process of oPD takes place in two steps: *i*) oPD monomer oxidizes to produce cation radical and *ii*) this radical is dimerized by coupling *via* C-N or C-C. After coupling, PoPD as ladder polymer bearing phenazine rings is successfully generated with oxidation of predominant head-to-tail structure dimers.^{42, 45} Likewise, electro-polymerization of oPD using cyclic voltammetry in previous studies have also exhibited analogous redox behavior.^{40, 46}

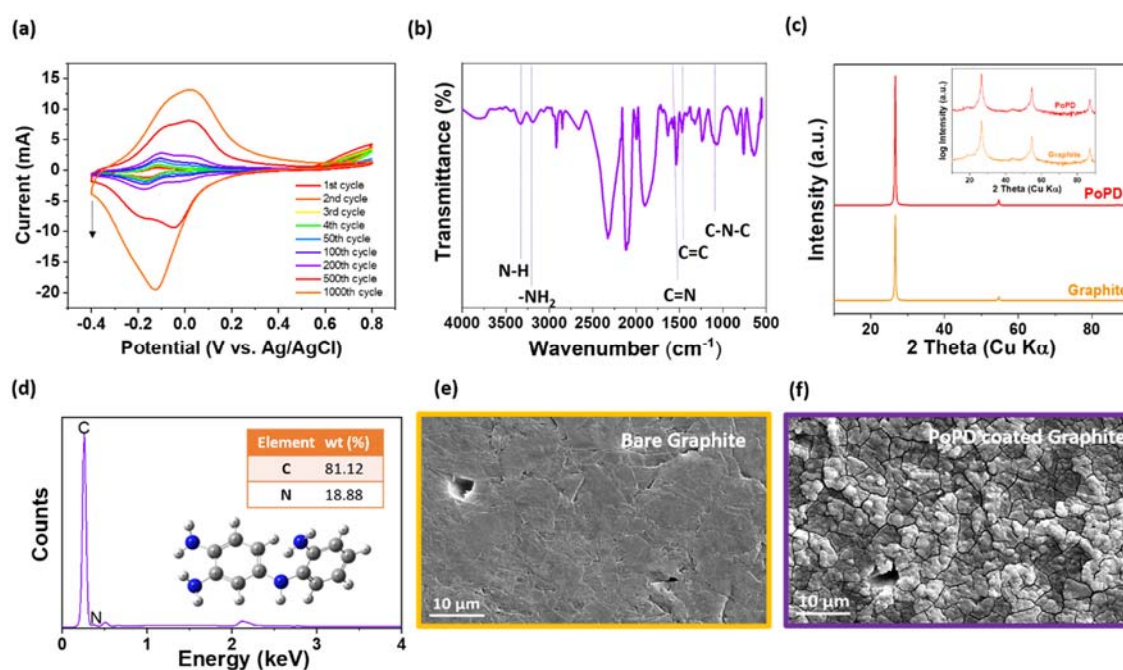


Figure 1: (a) CV curves during the electro-polymerization of oPD on graphite plate, (b) FTIR spectrum of PoPD electrode, (c) XRD patterns of graphite and PoPD electrode deposited on graphite plate, inset: XRD patterns of graphite and PoPD electrode with log intensities at the y-axis, (d) EDS analysis of PoPD electrode, inset image: proposed PoPD repeating unit, inserted from Figure S2, SEM images of (e) bare graphite plate and (f) PoPD electrode deposited on graphite plate.

Molecular structure of PoPD electrode was investigated by FTIR (Figure 1b). The representative peaks at 3324 cm^{-1} and 3180 cm^{-1} are ascribed to -NH- and -NH₂, respectively. Peaks in the region between 1700 to 3000 cm^{-1} attributed to atmospheric carbon dioxide⁴⁷ as well as those from the graphite substrate (Figure S1). Stretching of C=N and C=C vibrations were observed at the corresponding peaks at 1629 cm^{-1} and 1534 cm^{-1} , representing the successful electro-polymerization of oPD. The peak at 1075 cm^{-1} was attributed to the C-N-C band. The bands between 972-759 cm^{-1} were originated from wagging of C-H group (out-of-plane C-H bending), indicating the presence of aromatic benzene ring. Our findings are well consistent with the FTIR signature spectrum of electropolymerized PoPD film in the previous reports.^{23, 27, 42, 46, 48-49}

X-ray diffraction pattern of graphite and PoPD electrode are shown in Figure 1c. Well-defined sharp peaks at 26.6°, 54.7° and 87.1° corresponds to (002), (004) and (112) planes of graphite.⁵⁰ However, diffraction peaks corresponding to PoPD could not be detected, revealing its amorphous structure. EDS elemental spectrum of PoPD electrode demonstrated the presence of carbon and nitrogen (Figure 1d). Then, we tried to rationalize the molecular structure of PoPD repeating unit by using density functional theory (DFT) method (B3LYP) with 6-31G (d) basis set.⁵¹ Visualization was performed by Gaussian 09 program package. When we calculate the weight ratio according to the repeating units in the figure (Figure S2), for 1,4 substituted benzenoid-quinoid structure of PoPD, 79.13 % of C and 15.38 % of N were found. Thus, the weight ratio of C and N is in a good agreement with EDS elemental analysis (81.12 % for C and 18.88 % for N). Additionally, the penetration depth in EDS analyses is around few microns which then probes the C from the graphite substrate. Hence slightly more weight estimated for C can be assigned to the carbon originated from the graphite current collector. To the best of our knowledge, the real structure of PoPD is an open ring polymer with free amine groups. The open ring polymer structure that is estimated in Figure S2 is close to that demonstrated in the work of Samanta *et al.*⁵² which has investigated the polymerization process of oPD monomer in H₂SO₄ medium.

Turning to the morphological characterizations, comparing the SEM images of bare graphite (Figure 1e) and PoPD film coated graphite (Figure 1f), it can be concluded that bare graphite has smoother surface than that of covered with PoPD. Lumpy surface of PoPD confirms that it covers the surface of graphite plate uniformly after 1000 CV cycles during electro-polymerization process. These combined results attest the effective electro-polymerization of PoPD on the graphite plate.

3.2 Electrochemical characterization and performance tests of PoPD on graphite plates

Prior to the electrochemical tests, pH and ionic conductivity values were measured for both AlCl_3 and ZnSO_4 containing aqueous electrolytes. While the pH of the AlCl_3 solution is rather acidic and it decreases from pH 3.2 to 0.5 by changing the concentration from 0.25 M to 3.0 M (Figure 2a), pH of the ZnSO_4 solution ranges from 5.6 and 4.4 depending on the concentration of the ZnSO_4 solution (Figure 2b). The ionic conductivity values of both electrolytes behave also differently. The ionic conductivity of AlCl_3 solution is much higher than that of ZnSO_4 and reaches a maximum value at 1.5 M AlCl_3 concentration (187 mS cm^{-1}). The conductivity of ZnSO_4 solution ranges from 18 to 63 mS cm^{-1} when the salt concentration rises from 0.5 M to 3.0 M. With the aim of keeping the ionic conductivity of the electrolytes as close as possible, all electrochemical characterizations have been carried out with 0.25 M AlCl_3 (pH 3.34) and 1 M ZnSO_4 (pH 5.16) aqueous solution with almost similar ionic conductivities of 49.6 mS cm^{-1} and 50 mS cm^{-1} , respectively (Figure 2a and b). Two metal salts with the same anion were not conceivable to eliminate the interference of anions on the charge storage mechanism of the PoPD electrode for several reasons. The ZnCl_2 (anhydrous) was not favored because it forms zinc oxychlorides upon dissolution in water leading to a turbid solution and some precipitation.⁵³ Even though those precipitations can be simply eliminated by the use of a few drop of HCl addition, addition of acid solution changes the pH along with the entire charge storage mechanism due to the altered $\text{Zn}^{2+}/\text{H}^+$ ratio in the electrolyte. Another point is the limitation of the EQCM measurement in a turbid solution (which would prevent the QCM working as a gravimetric probe, as discussed in Part 3.3). Therefore, a correlation

between the interface property and performance would not be possible in ZnCl_2 solution. The reason why $\text{Al}_2(\text{SO}_4)_3$ was not favored is related with (i) the extremely acidic nature of the resulting solution that causes damage on the substrates and (ii) its low ionic conductivity⁵⁴ that resulted in a very poor cycling performance (data now shown). Consequently, due to their superiority in different aspects, AlCl_3 and ZnSO_4 electrolytes were chosen as multivalent charge carriers to study the charge storage mechanism of the PoPD electrode, over $\text{Al}_2(\text{SO}_4)_3$ and ZnCl_2 solutions.

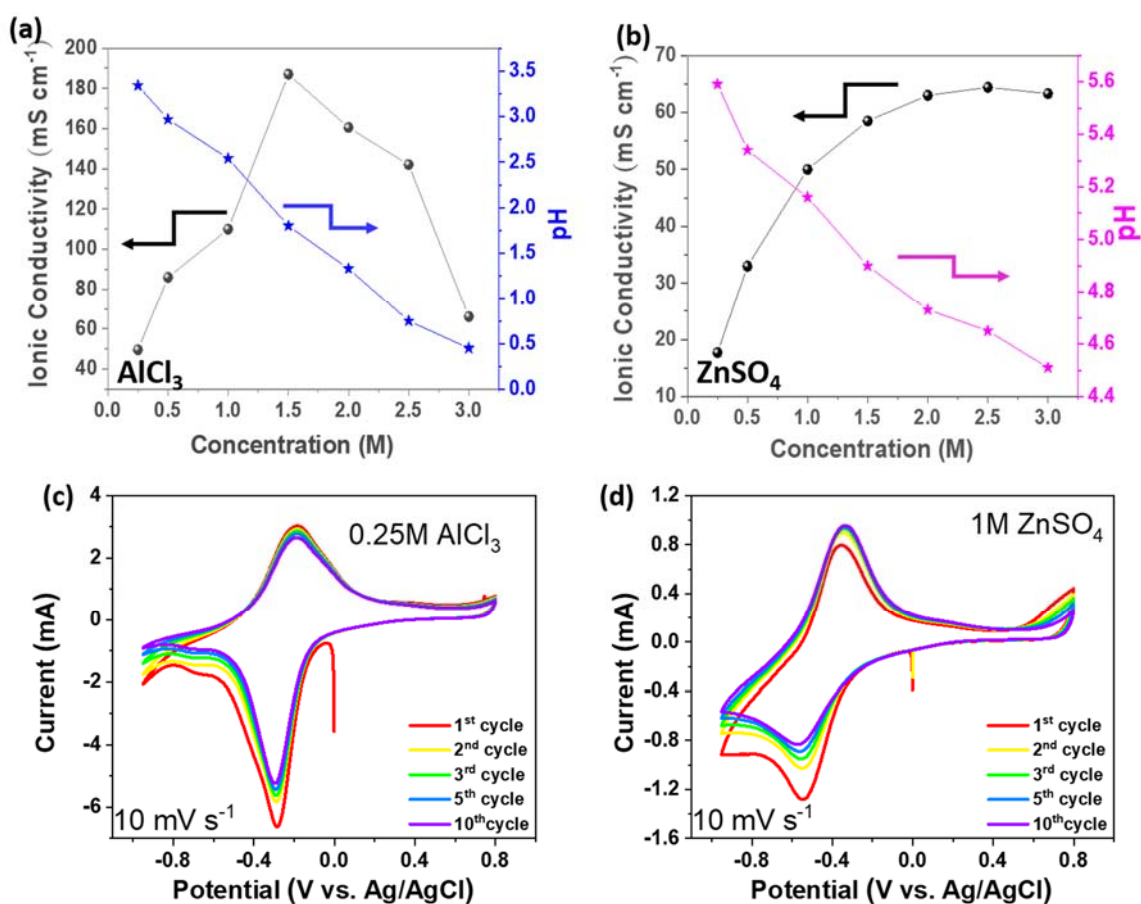


Figure 2: Ionic conductivity and pH of the different electrolyte concentration of (a) AlCl_3 and (b) ZnSO_4 . CV curves of PoPD on graphite electrodes at a scan rate of 10 mV s^{-1} in (c) 0.25 M AlCl_3 electrolyte and in (d) 1 M ZnSO_4 electrolyte.

To investigate the electrochemical behavior of PoPD, deposited on graphite plates, in the two different aqueous electrolytes, CV was initially carried out in 0.25 M AlCl_3 and 1 M ZnSO_4 at a scan rate of 10 mV s^{-1} between -0.95 and 0.8 V vs. Ag/AgCl. The CV curves of PoPD in aqueous AlCl_3 electrolyte exhibit a

cathodic peak at -0.28 V and an anodic peak at -0.19 V during the first reduction and oxidation cycle, respectively. Throughout subsequent cycles, similar electrochemical response was observed, which can be attributed to a reversible and fast electrochemical process into/from PoPD electrode (Figure 2c). On the other hand, cyclic voltammograms of PoPD in 1 M ZnSO₄ aqueous solution exhibit one cathodic peak at -0.55 V and one anodic peak at -0.35 V (Figure 2d), which may signify insertion/extraction of ions into/from active side of PoPD electrode. The slight difference in the peak position of the redox couple obtained in Al³⁺ and Zn²⁺ containing electrolytes could be assigned to the different hydration radius and ionic hydration energies of the corresponding cations.⁵⁵

The galvanostatic discharge/charge performance of PoPD electrode in aqueous electrolytes of 1 M ZnSO₄ and 0.25 M AlCl₃ has been investigated at different current densities in three-electrode configuration. As seen in Figures 3a and 3b, the discharge/charge profiles demonstrate an average voltage of around -0.40 V in 1 M ZnSO₄ and -0.20 V in 0.25 M AlCl₃, which are in well agreement with the CV results. PoPD electrode in 1 M ZnSO₄ delivered average discharge capacities of around 32, 42, 58, 70 and 112 mAh g⁻¹ (Figure 3c), while in 0.25 M AlCl₃, 213, 122, 127, 131 and 156 mAh g⁻¹ discharge capacities were obtained at the current densities of 20 C, 15 C, 10 C, 8 C and 5 C, respectively (Figure 3d), demonstrating that PoPD electrode exhibited a better rate performance in 0.25 M AlCl₃ electrolyte. Improved rate capability in AlCl₃ compared with its Zn counterpart and the reasons behind this dissimilar performance have further been probed with ion transport and interfacial ion transfer analyses with EIS and EQCM, respectively (Section 3.3). Moreover, the long-term cycling performance of PoPD was assessed at the same current density (5C) in both electrolytes. As depicted in Figure 3e, PoPD delivered an initial discharge capacity of 379 mAh g⁻¹ in 0.25 M AlCl₃ and after 1000 cycles a capacity of 110 mAh g⁻¹ was obtained with a capacity retention of 56 %. Figure 3f illustrates the cycling performance in 1 M ZnSO₄ that PoPD exhibited the first discharge capacity of 143 mAh g⁻¹ in 1 M ZnSO₄, and retained its discharge capacity of 93 mAh g⁻¹ after 1000 cycles.

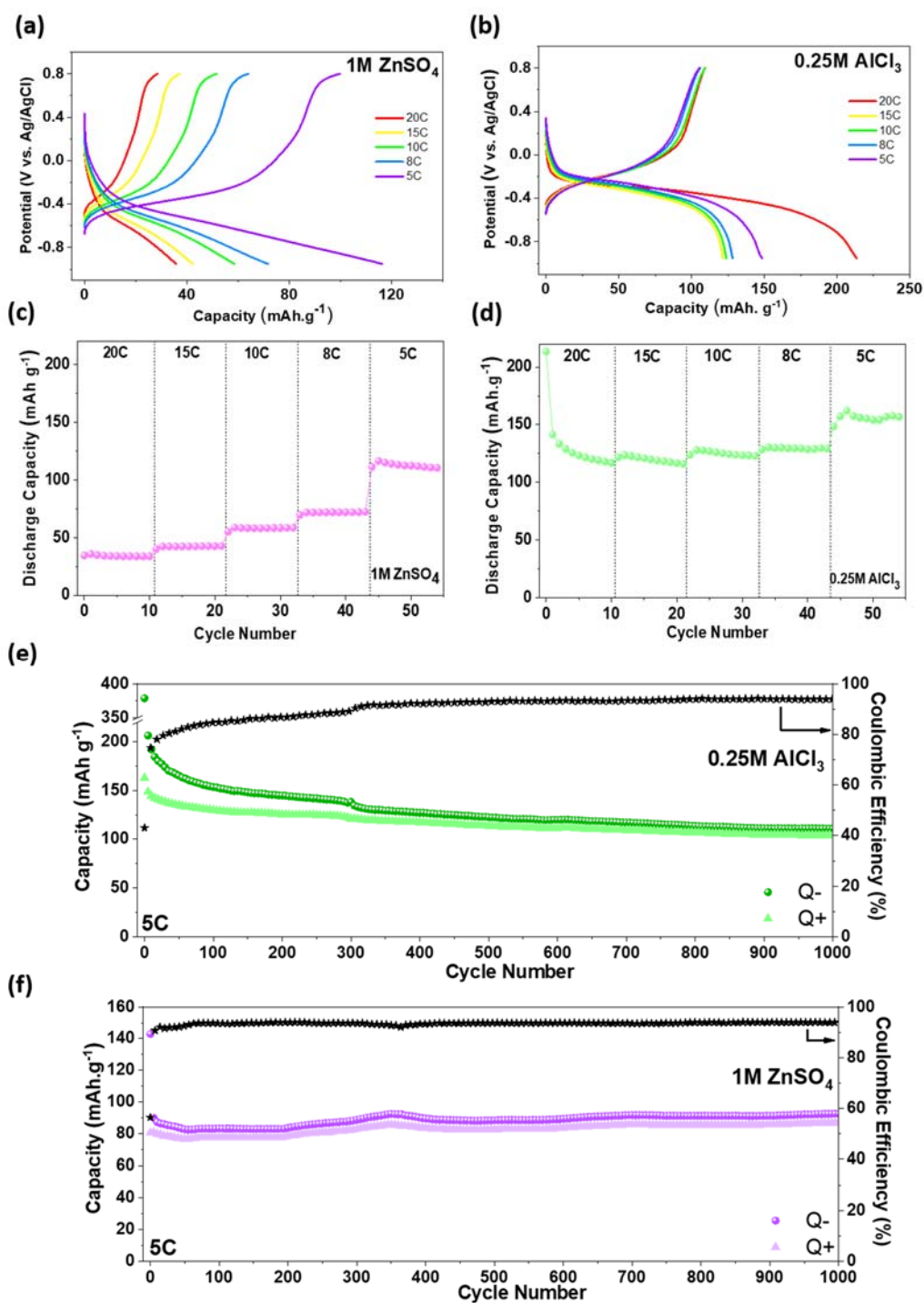


Figure 3: Electrochemical performance of PoPD. Discharge/charge plateau at different current densities in (a) 1 M ZnSO₄ aqueous electrolyte and (b) 0.25 M AlCl₃ aqueous electrolyte. C-rate performances in (c) 1 M ZnSO₄ and (d) 0.25 M AlCl₃. Long term-cycling performances at a current density of 5C in (e) 0.25 M AlCl₃ and (f) 1 M ZnSO₄.

The structural stability of the PoPD electrodes after long-term cycling process was shown with the SEM analysis in Figure S3. In comparison with the pristine electrode, there is almost no visible changes observed, revealing their structural integrity. Parasitic reactions in aqueous electrolyte such as the hydrogen evolution and presence of dissolved oxygen,^{6, 56} result lower Coulombic efficiencies (CE) and subsequent partial irreversible discharge/charge process in both electrolytes. Moreover, proton uptake/removal rather than zinc has already been reported in ZIBs with organic polymer electrode containing phenazine nitrogen atoms.⁵⁷ In aqueous Al^{3+} containing electrolytes, a recent study reported the aluminum ions' role in the redox process of PANI electrode, in addition to the proton insertion/(de)insertion and anion (de)doping.²¹ In comparison with the other organic electrode materials employed in aqueous electrolyte zinc-ion battery systems, the PoPD conductive polymer as a candidate of organic electrodes exhibited high rate and good cycling performance (Table S1). Notably, organic electrode materials composed of small molecules, macromolecules, or polymeric molecules (through a variety of relatively weak intermolecular interactions such as van der Waals forces, hydrogen bonds, π - π interactions, and electrostatic Coulomb forces¹¹) are appealing due to their flexibility, environmental friendliness, and the tunable molecular structure. Thus, their zinc ion storage performances have been investigated.¹² However, PoPD electrode was used for the first time in an aluminum-containing aqueous electrolyte in our study. It is noted that compared with the other organic electrodes (Table S2), it provides high capacity at high current density.

Regarding the CE, even though values were later improved, initially lower CE values were obtained (Figure 3) due to the significant imbalance between the potential proton insertion/(de)insertion by PoPD electrode. In order to further understand the role of proton on the CE values, electrochemical performance of PoPD in 0.25 M AlCl_3 +HCl electrolyte (pH=1.54, ionic conductivity=56 mS cm^{-1}) was tested. As depicted in Figure S4a, PoPD electrode in 0.25 M AlCl_3 +HCl electrolyte exhibited the first discharge capacity of 632 mAh g^{-1} and after 50 cycles discharge capacity decreased to 204 mAh g^{-1} with 85% Coulombic efficiency (CE). Thus, dual carrier insertion process improves the electrochemical performance of PoPD

electrode. On the other hand, the CE of PoPD in AlCl_3+HCl electrolyte is even lower than that in pristine AlCl_3 electrolyte demonstrating the impact of the protons on the CE (Figure S4b) that is in an agreement with a literature report.⁵⁸

Better electrochemical performance of PoPD electrode in 0.25 M AlCl_3 electrolyte compared to that in 1 M ZnSO_4 is considered to be related to the hydration-radius and the dehydration energy of the ion participating in the charge compensation process. Considering a charge compensation occurring with dehydrated cations, the ionic radius of Al^{3+} (0.5 Å) is relatively smaller than that of Zn^{2+} ions (0.74 Å), which is beneficial to acquire a fast ion transfer and advanced rate capability. Taking into account the hydrated radius, hydrated Al^{3+} (1.87- 1.90 Å) (aluminum could be the octahedral form of $\text{Al}(\text{H}_2\text{O})_6^{3+}$ in acidic media)⁵⁹⁻⁶⁰ is also smaller than that of hydrated Zn^{2+} (4.3 Å).⁵ As a result of partial dehydration of the octahedral unit of aluminum ($\text{Al}(\text{H}_2\text{O})_6^{3+} \leftrightarrow \text{Al}(\text{OH})(\text{H}_2\text{O})_5^{2+} + \text{H}^+$), proton and hydrated aluminum ion with a smaller hydration number are formed, thus proton intercalation into host material could be also plausible.⁵⁹ Moreover, the hydration shell of Zn^{2+} containing six water molecules, is one of the challenging factor to be accommodated in the host structure,⁶¹ thus slower kinetics in the case of zinc insertion could be expected. EQCM analyses in Section 3.3 have been employed to investigate the nature of the ions dominating the charge storage process.

3.3 Investigation of the dissimilarity of performance behavior in AlCl_3 and in ZnSO_4 electrolytes

To analyze the charge storage mechanism of PoPD electrode in both electrolytes, CV analyses at various scan rates of 1, 5 and 10 mV s^{-1} (Figures S5a and S5c) were conducted. The relationship between $\log(i)$ vs. $\log(v)$ (where v is the potential scan rate) (Figures S5b and S5d) and the detail of the calculation can be found in supporting information Part E. Then, the contribution of the capacitive and diffusion controlled process was estimated according to the following expression:⁶²

$$i(V) = k_1 v + k_2 v^{1/2} \quad (\text{Equation 1})$$

where the term of $k_1 v$ represents capacitive contribution and the other term of $k_2 v^{1/2}$ corresponds to the effect of diffusion-controlled process. According to Equation 1, k_1 is the slope and k_2 is the intercept of the $i/v^{1/2}$ vs $v^{1/2}$ curve (data not shown). As depicted in Figure S6, PoPD demonstrates 59 % and 62 % of capacitive contribution in 1 M ZnSO₄ and 0.25 M AlCl₃ at a sweep rate of 1 mV s⁻¹, respectively and the ratio of capacitive contribution gradually increases, as expected, with the rising sweep-rates. The mutual contribution of the surface and bulk processes indicates the pseudocapacitive behavior of PoPD electrodes in both electrolytes.

Although PoPD exhibits similar capacitive and diffusion-controlled behavior in both Zn and Al containing electrolyte, to further evaluate the ion transport mechanism during the electrochemical performance, PoPD electrodes were investigated by EIS in 0.25 M AlCl₃ and 1 M ZnSO₄ aqueous electrolytes, before and after C-rate tests. Figure S7 shows that Nyquist plots of PoPD electrodes in 1 M ZnSO₄ and 0.25 M AlCl₃ exhibit depressed semicircles associated with the charge transfer process, followed by a straight line with a slope of 45° arising due to Warburg impedance in the low frequency region.⁶³ As was shown in Equations S2 and S3 in supporting information file, ion diffusion coefficient and Warburg coefficient can be calculated from the Warburg impedance.⁶⁴ Warburg coefficients were obtained from the linear fit of the plot of Z' vs. $\omega^{-0.5}$ for 1 M ZnSO₄ and 0.25 M AlCl₃ aqueous electrolytes illustrated in Figures S8 and S9, respectively. Since the slope of the curve is much lower in Al³⁺ containing electrolyte than that of Zn²⁺, both before and after cycling, one could conclude that faster ion diffusion in PoPD electrode takes place in AlCl₃ containing electrolyte than that of ZnSO₄.

In a next step, EQCM-based analyses were performed to investigate the charge storage mechanism and the dissimilar performance behavior of PoPD in Al³⁺ and Zn²⁺ containing electrolytes. Figure 4a depicts the CV response along with the microbalance frequency variation of PoPD film in 1 M ZnSO₄ solution. The direction of the sweep has been highlighted with the arrows. Pair of redox peaks situated at -0.5 V and -0.3 V vs. Ag/AgCl can be observed in the CV profile which is well consistent with the Figure 2d and the reported literature.³⁹ A prominent frequency decrease and increase take place during the reduction

and oxidation, respectively. This signifies either the electro-adsorption/desorption or insertion/deinsertion of the charged species into the PoPD framework, assuming that the microbalance works under the gravimetric regime. The term 'gravimetric regime' is used to describe the conditions where the frequency changes can be converted to the mass changes, according to Sauerbrey equation, which is applicable to thin dense films with flat surface rigidly attached to the quartz resonators' surface (in the absence of solid-liquid hydrodynamic interactions and without any changes in the viscoelastic properties).²⁹⁻³⁰ The beginning and end of the frequency variation overlap in Figures 4a and 4c, which indicates the reversibility of the process. The hysteresis in frequency response is assumed to be due to the differences between the kinetic rates of the interfacial species transfer which occurs during the discharge/charge process.⁶⁵⁻⁶⁶ The stability of the film has been probed with the frequency, charge and current variation with time (Figure 4b), no significant decay was observed except a slight upward trend in the frequency profile. Figure 4a shows the respective data after stabilization of the current. For PoPD film cycled in AlCl_3 solution, prominent reduction and oxidation peaks can be observed at -0.2 V and -0.15 V *vs.* Ag/AgCl, respectively (Figure 4c). The frequency variation follows the similar trends like its Zn counterpart, *i.e.*; frequency decrease/increase during a cathodic/anodic scan as shown in Figure 4c. However, unlike Zn, the magnitude of frequency variation observed in this case is much smaller. It is noted that the PoPD films used for tests in ZnSO_4 and AlCl_3 have similar loadings (electrodeposited under the same conditions, leading to a thickness of $\sim 150 \text{ nm}^{40}$), therefore the significant difference in Δf response indicates an alteration of the interfacial processes which is interpreted considering different aspects, *i.e.* the nature of the (de)inserted ions, the role of protons and additional surface layer formation. The EQCM response of subsequent cycles has also been shown for the AlCl_3 electrolyte (Figure 4d) and a reasonable stability over the cycles is observed.

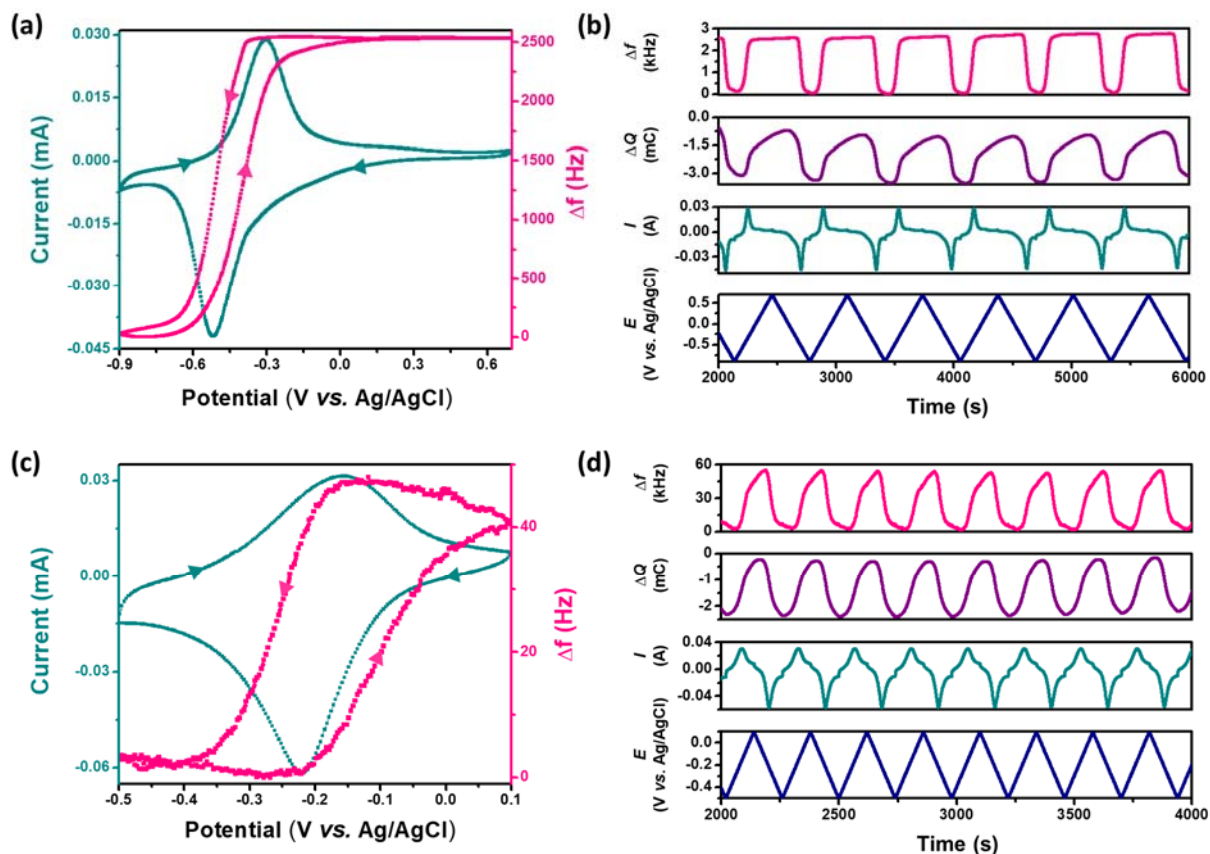


Figure 4: Cyclic voltammogram and microbalance frequency response of PoPD films in (a) 1 M ZnSO_4 electrolyte and (c) 0.25 M AlCl_3 carried out at 5 mV s^{-1} ; Frequency, charge, current and potential as a function of time for (b) 1 M ZnSO_4 and (d) 0.25 M AlCl_3 electrolyte.

Here, we assume that the film is thin enough and strongly attached to the gold electrode of the QCM which enables us to apply Sauerbrey equation⁴¹ under gravimetric regime to convert the Δf into Δm and estimate mass per electron (MPE) values. If the charge transfer process is dominated by only one species, the MPE would be equivalent to its molar mass. To estimate the MPE value, Δm has been plotted as a function of charge variation (ΔQ) and MPE has been calculated from the slope ($\frac{\Delta m}{\Delta Q}$). The corresponding profile of PoPD film cycled in ZnSO_4 during reduction and oxidation have been depicted in Figure 5a and Figure 5b, respectively. During reduction (Figure 5a), the two different regions (highlighted with shaded area) with lower and higher MPE_{exp} values than that of $\text{MPE}(\text{Zn}^{2+})$ (*i.e.*, 32.7 g mol^{-1}) have been noticed. During the oxidation, the MPE_{exp} (or the slope ($\frac{\Delta m}{\Delta Q}$)) is also significantly higher than that of theoretical

(Figure 5b). On the other hand, in case of AlCl_3 electrolyte, the MPE values calculated from the mass *vs.* charge variation are smaller than the MPE of Al^{3+} (*i.e.*; 9 g mol^{-1}) during both reduction and oxidation (Figure 5c and 5d). The theoretical MPE values of Zn^{2+} and Al^{3+} have been highlighted with brown straight line in respective plots.

It can be observed that in none of the case, the MPE values are in well agreement with the respective cations, especially for Zn^{2+} , the mass variation is vast. To investigate this enormous mass variation, the motional resistance changes (ΔR_m) has also been monitored along with the microbalance frequency and current. Figures S10a and S10b depict the variation of microbalance frequency and motional resistance with time in ZnSO_4 and AlCl_3 solution, respectively. The estimated $\frac{\Delta R_m}{\Delta f}$ gives a maximum value around $0.05 \Omega \text{ Hz}^{-1}$ for ZnSO_4 and higher than that in AlCl_3 electrolyte (for the latter the ΔR_m is rather small). Figure 5a exhibits a low experimental MPE value during the onset of the reduction process indicates the insertion of Zn^{2+} and/or hydrated proton in the PoPD framework, which has been highlighted in green. This highlighted region is shown separately in supporting information (SI) along with the frequency and motional resistance variation (Figures S11a and S11b). At the onset of reduction, the low MPE (-12 g mol^{-1}) induces small increase in the motional resistance (Figure S11b). Whereas, at the reduction peak, the large MPE suggests species heavier than Zn^{2+} is involved, which is supported with the enormous increase in the motional resistance shown in Figure S11b that is an enlarged version from Figure S10a. This substantial Δf and ΔR_m can be addressed by the well-known $\text{Zn}_4(\text{OH})_6\text{SO}_4 \cdot n\text{H}_2\text{O}$ (ZHS) formation during the reduction process at the electrode-electrolyte interface, reported in several literature.⁶⁷⁻⁷¹ The ZHS formation can increase the local viscosity at the interface which can perturb the microbalance from functioning as a gravimetric probe. During oxidation, again a MPE value greatly higher than that of Zn^{2+} is obtained, and assumed to be a combined contribution from de-insertion of $\text{Zn}^{2+}/\text{H}_3\text{O}^+$ as well as dissolution of ZHS (Figure 5b). It is emphasized that in Figure 5 the MPE values are only given for the regions where the ΔR_m values are small, so that the Sauerbrey equation can be applied. The higher slope

$(\frac{\Delta m}{\Delta Q})$ regions (Figure 5a, b, highlighted with pink background) are interpreted considering the ZHS formation/dissolution intervening in the ion intercalation-deintercalation process and the EQCM-R (R_m monitoring) is used as a qualitative characterization tool for the ZHS formation.⁷² The ΔR_m values are remarkably reversible (*i.e.*; increase during a cathodic sweep and decrease to initial value on the reverse scan) indicating that the complete dissolution of the ZHS at the end of charge.

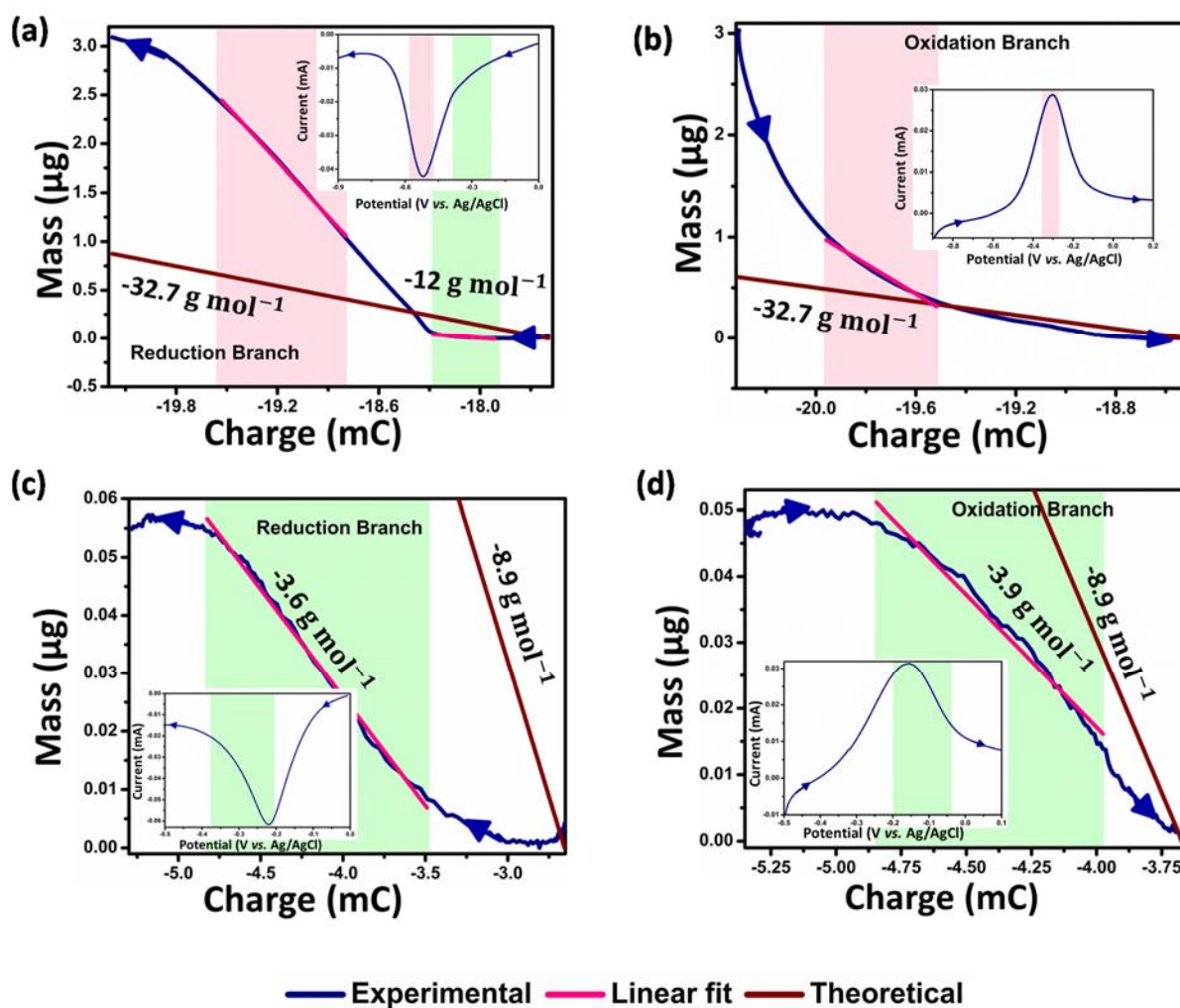


Figure 5: Electrode mass *vs.* charge change during reduction and oxidation, shown for 1 M ZnSO_4 (a and b) and 0.25 M AlCl_3 (c and d), respectively. The voltage ranges corresponding to the linear fit in (a to d) have been estimated from the different slopes in the mass *vs.* charge profile.

Along with the EQCM measurements, EDS analyses and *ex-situ* X-ray diffraction tests were performed in order to investigate the ZHS formation of the PoPD electrodes at the end of the 1st discharge. EDS spectra depicted in Figures S12a and S12b demonstrate that while there are sharp peaks appeared at the PoPD electrode in Zn containing electrolyte belonging to the Zn, S and O elements, almost no change were observed in AlCl₃. Although both PoPD electrodes were washed with bi-distillated water, the additional peaks appeared on the surface of the electrode in ZnSO₄ could be assigned to the formation of flake shaped ZHS (Zn₄SO₄(OH)₆·5H₂O) structure which is a well-known morphology of zinc sulfate hydroxide⁷³. Moreover, EDS mapping of pristine PoPD electrode demonstrates the homogeneous distribution of nitrogen and carbon elements on graphite substrate (Figure S13a). Figure S13b verified the locally covered Zn on the PoPD electrode after fully discharged. The Zn/S mole ratio around 2.5 (calculated from the EDS wt% in Figure S12a) was obtained that is sufficiently close to the ZHS composition. Later, *ex-situ* XRD measurements confirmed the presence of a peak at around 9° corresponding to Zn₄SO₄(OH)₆·5H₂O formation after the first discharged state of the PoPD electrode in 1 M ZnSO₄ (Figure 6a, b). Furthermore, in order to elucidate the proton insertion into PoPD, time dependent FTIR analyses (Figure 6c, d) were performed during the first discharge/charge states in 1 M ZnSO₄ electrolyte at a current density of C/2. In the FTIR spectra, it was evident that the most significant intensity variation occurred at 3324 cm⁻¹ corresponds to N-H bond, the intensity of N-H slightly increased during the discharge, and decreased during the charge state, indicating plausible reversible proton insertion.⁵⁷

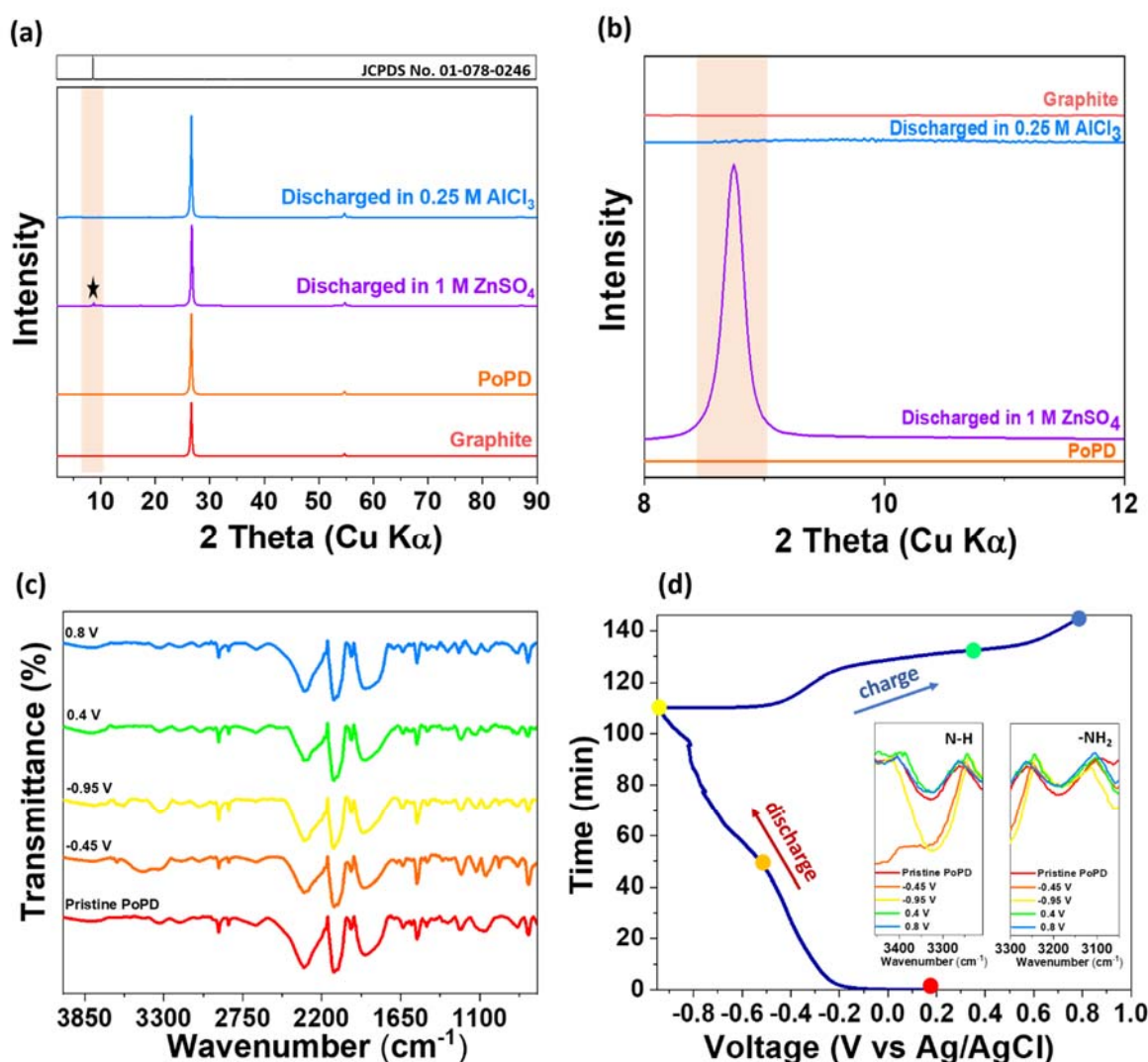


Figure 6: (a) XRD of graphite, PoPD electrode, PoPD at the end of the discharged in 1 M ZnSO₄ and 0.25 M AlCl₃, (the star symbol demonstrates the characteristic diffraction peak of the formed ZHS) (b) XRD peak analysis zoomed between 8° and 12°. (c) FTIR spectra of PoPD electrode at the pristine and different voltage, (d) time-voltage profile of PoPD in 1 M ZnSO₄ electrolyte and inset images show the peaks of the FTIR spectra between wavenumbers of 3500 and 3000 cm⁻¹.

Unlike the Zn system (Figure S10a), a minor variation of motional resistance in AlCl₃ electrolyte (Figure S10b) indicates that the (de)intercalation of ionic species into the cathode framework does not cause a deviation from the gravimetric regime of the EQCM. Although the calculated MPE values are greater than that of MPE (Zn²⁺) (*i.e.*, 32.7 g mol⁻¹) in the previous system, except on the onset of the reduction peak

(Figure 5a), for AlCl_3 electrolyte, the calculated MPE (-3.6 and -3.9 g mol^{-1} for cathodic and anodic scan, respectively) is lower than theoretical MPE of Al^{3+} (Figures 5c and 5d). This gives an indication that the Al^{3+} species might not be the dominant ionic species and other ions (with different valence and molar mass) may take part in the charge compensation process.

To quantify the partial contribution of the multivalent cations, the charge fraction ($x = Q_{\text{Al}^{3+}}/\Delta Q$) has been calculated considering Al^{3+} and H_3O^+ are the ionic species taking part in the redox reaction according to the following equation:⁷⁴

$$\Delta f = \frac{-k_s}{A.F} \left[\frac{x(\Delta Q * M_{\text{Al}^{3+}})}{n_{\text{Al}^{3+}}} + \frac{(1-x)(\Delta Q * M_{\text{H}_3\text{O}^+})}{n_{\text{H}_3\text{O}^+}} \right] \quad (\text{Equation 2})$$

where Δf is the microbalance frequency variation, k_s is the experimental sensitivity coefficient ($16.3 \times 10^7 \text{ Hz g}^{-1} \text{ cm}^2$), $A = 0.2 \text{ cm}^2$ is the active area of quartz and F is the Faraday constant, ΔQ is the charge variation, $M_{\text{Al}^{3+}}$, $n_{\text{Al}^{3+}}$, $M_{\text{H}_3\text{O}^+}$ and $n_{\text{H}_3\text{O}^+}$ represents the molar mass, and the number of transferred electrons by Al^{3+} and hydrated protons, respectively. The charge fraction $x = \frac{Q_{\text{Al}^{3+}}}{\Delta Q}$ denotes the fraction of charge compensated by the Al^{3+} out of the total charge variation. The calculated charge fraction for Al^{3+} ($x = \frac{Q_{\text{Al}^{3+}}}{\Delta Q}$) is 0.16 ($\frac{Q_{\text{H}_3\text{O}^+}}{\Delta Q}$ is 0.84) and it is well consistent with the MPE analysis. Recent literature also demonstrates that in acidic pH, protons are more likely to participate in the charge compensation than the respective cations present in the electrolyte used.⁷⁵⁻⁷⁶ A similar estimation can be possible for ZnSO_4 electrolyte but for a more restricted potential range. In Figure S11a, green portion where the absolute value of MPE is 12 g mol^{-1} , corresponds to a $\frac{Q_{\text{Zn}^{2+}}}{\Delta Q}$ value of 0.40 over $\frac{Q_{\text{H}_3\text{O}^+}}{\Delta Q}$ value of 0.60 . This suggests that a more significant contribution of H_3O^+ in the charge compensation process in AlCl_3 than that happens in ZnSO_4 electrolyte. This dissimilarity in the proportion of the ionic species transferred at the electrode/electrolyte interface may also govern the ionic diffusion in the bulk of the electrode. Although the experiments cannot be directly comparable with the film thickness on graphite electrode, the result

obtained with EQCM is still well consistent with the Warburg coefficient estimations in Figures S8 and S9, where a higher diffusion coefficient was estimated in case of AlCl_3 electrolyte, as $\text{H}_3\text{O}^+/\text{Al}^{3+}$ ratio is higher than that of $\text{H}_3\text{O}^+/\text{Zn}^{2+}$. For the ZnSO_4 electrolyte, a relatively smaller portion of Zn^{2+} is replaced by H_3O^+ and the additional effect of the evolution of the interface with the ZHS formation make the ion diffusion slower than that happens in AlCl_3 . It has been reported that local change in the pH value resulting from potential proton involvement in the charge compensation process promotes ZHS formation in which at a pH of 5.47 ZHS formation initiates.⁷⁷ For the present EQCM-R analysis, the ZHS formation is responsible for the enormous frequency and motional resistance change during cycling. It does not take part in the charge compensation process but our comparative results obtained in AlCl_3 and ZnSO_4 electrolytes show that it can affect the ions' interfacial transfer and transport properties. Scheme 1 also demonstrates an illustration of the dissimilar behavior of PoPD in the different electrolytes.

4. Conclusion

Herein, the charge storage performance and interfacial processes occurring at an organic electrode interface, in two different electrolytes containing Zn^{2+} and Al^{3+} multivalent ions were investigated. Among the CP electrodes, a relatively less investigated aromatic diamine-based CP, *i.e.*, PoPD has been studied in detail. The Al/PoPD cell has exhibited better cycling stability with a discharge capacity of 110 mAh g^{-1} after 1000 discharge/charge cycles at a current density of 5C than that of Zn/PoPD cell. The plausible reason behind this difference has been probed from different aspects. While the ratio of the capacitive to diffusion-controlled process seems to be unaltered in both electrolytes, the diffusion coefficient estimated from EIS analyses indicated that faster ion diffusion in PoPD electrode takes place in AlCl_3 containing electrolyte compared to its Zn counterpart. Thus, the challenging task of finding out the nature of these ions was undertaken by EQCM analyses. It revealed a significant contribution of the H_3O^+ in the charge compensation process, in addition to the respective multivalent ions. Especially, in the case of AlCl_3 , it is evident that the contribution of protons dominates over Al^{3+} . No anion participation is noticed in both

electrolytes. Proton involvement was further verified by time-dependent FTIR with PoPD electrode cycled in ZnSO_4 electrolyte through the observation of the -NH groups. Later, *ex-situ* XRD measurement revealed the well-known ZHS formation at the end of the discharged state due to the proton insertion accompanied by the local pH increase. Additionally, EQCM explored the formation/dissolution of ZHS at electrode-electrolyte interface during reduction/oxidation, and the motional resistance increase was observed only in ZnSO_4 electrolyte not for AlCl_3 electrolyte. To the best of our knowledge, this work is the first report elucidating the nature of charge carries of an organic electrode, PoPD, in a comprehensive/comparative manner in which both $\text{Al}^{3+}/\text{Zn}^{2+}$ ion and H_3O^+ as co-ions reversibly intercalate/(de) intercalate into/from the PoPD film. Besides the differences of the size of the Al^{3+} or Zn^{2+} species, the better cycling stability and a higher discharge capacity in aqueous AlCl_3 than that in ZnSO_4 seem to be related to the ZHS formation in the latter electrolyte, which is known to hinder the ion transport, as revealed by EIS analysis of this study. As a whole, PoPD organic electrodes exhibited high-rate capability and excellent cycling stability performance in aqueous electrolyte multivalent systems with a tendency for a better performance in AlCl_3 electrolyte revealing the role of both electrolyte cations as well as non-negligible participation of protons in the charge storage mechanism.

ASSOCIATED CONTENT

Supporting Information. Additional characterization data of PoPD electrodes. Electrochemical tests on the role of proton for the CE values. EDS analyses, XRD measurement and time dependent FTIR spectra of the cycled PoPD electrodes, additional EIS data analyses and EQCM data with motional resistance monitoring.

AUTHOR INFORMATION

Corresponding authors

Rezan Demir-Cakan; *Gebze Technical University, Department of Chemical Engineering, 41400 Gebze, Kocaeli, Turkey*

Email: demir-cakan@gtu.edu.tr

Ozlem Sel; *Sorbonne Université, CNRS, Laboratoire Interfaces et Systèmes Electrochimiques, LISE, 75005 Paris, France*

Email: ozlem.sel@sorbonne-universite.fr

Authors:

Selin Sariyer; *Gebze Technical University, Department of Chemical Engineering, 41400 Gebze, Kocaeli, Turkey*

Arpita Ghosh; *Sorbonne Université, CNRS, Laboratoire Interfaces et Systèmes Electrochimiques, LISE, 75005 Paris, France*

Sevde Nazli Dambasan; *Gebze Technical University, Department of Chemical Engineering, 41400 Gebze, Kocaeli, Turkey*

El Mahdi Halim; *Sorbonne Université, CNRS, Laboratoire Interfaces et Systèmes Electrochimiques, LISE, 75005 Paris, France and University of Hassan II of Casablanca, Faculty of Sciences and Technology, Laboratory of Materials, Membranes and Environment -BP 146, 20650 Mohammedia, Morocco*

Mama El Rhazi; *University of Hassan II of Casablanca, Faculty of Sciences and Technology, Laboratory of Materials, Membranes and Environment -BP 146, 20650 Mohammedia, Morocco*

Hubert Perrot; *Sorbonne Université, CNRS, Laboratoire Interfaces et Systèmes Electrochimiques, LISE, 75005 Paris, France*

Notes

The authors declare no competing financial interest.

ACKNOWLEDGMENTS

This work is partially supported by the TUBITAK- France PIA Bosphorus Bilateral project (project no: 119N054). The authors acknowledge the financial support and laboratory facilities of the Gebze Technical University and LISE UMR8235, Sorbonne University, CNRS. RDC is thankful to the French Embassy for the Visiting Researcher Fellowship and Labex MATISSE visiting professor programme (Sorbonne University). AG and OS acknowledges Sorbonne University-Emergence project for the financial support. Burcu Unal is thanked for the fruitful discussion. Hatice Yasemin Iskender is acknowledged for the EDS analyses. We would like to thank TUBITAK ULAKBIM, High Performance and Grid Computing Center (TR-Grid e-Infrastructure) for the calculations of the data in the computational chemistry details of this manuscript. Nazmiye Kılıç is thanked for her assistance in computational chemistry.

REFERENCES

- (1) Ghosh, S.; Maiyalagan, T.; Basu, R. N. Nanostructured conducting polymers for energy applications: towards a sustainable platform. *Nanoscale* **2016**, *8* (13), 6921-6947, DOI: 10.1039/c5nr08803h.
- (2) Yang, J.; Liu, Y.; Liu, S. L.; Li, L.; Zhang, C.; Liu, T. X. Conducting polymer composites: material synthesis and applications in electrochemical capacitive energy storage. *Materials Chemistry Frontiers* **2017**, *1* (2), 251-268, DOI: 10.1039/c6qm00150e.
- (3) Selvakumaran, D.; Pan, A. Q.; Liang, S. Q.; Cao, G. Z. A review on recent developments and challenges of cathode materials for rechargeable aqueous Zn-ion batteries. *J. Mater. Chem. A* **2019**, *7* (31), 18209-18236, DOI: 10.1039/c9ta05053a.
- (4) Demir-Cakan, R.; Palacin, M. R.; Croguennec, L. Rechargeable aqueous electrolyte batteries: from univalent to multivalent cation chemistry. *J. Mater. Chem. A* **2019**, *7* (36), 20519-20539, DOI: 10.1039/c9ta04735b.
- (5) Chao, D. L.; Zhou, W. H.; Xie, F. X.; Ye, C.; Li, H.; Jaroniec, M.; Qiao, S. Z. Roadmap for advanced aqueous batteries: From design of materials to applications. *Science Advances* **2020**, *6* (21), DOI: 10.1126/sciadv.aba4098.
- (6) Elia, G. A.; Kravchyk, K. V.; Kovalenko, M. V.; Chacon, J.; Holland, A.; Wills, R. G. A. An overview and prospective on Al and Al-ion battery technologies. *Journal of Power Sources* **2021**, *481*, DOI: 10.1016/j.jpowsour.2020.228870.
- (7) Tang, B. Y.; Shan, L. T.; Liang, S. Q.; Zhou, J. Issues and opportunities facing aqueous zinc-ion batteries. *Energy & Environmental Science* **2019**, *12* (11), 3288-3304, DOI: 10.1039/c9ee02526j.
- (8) Zhang, K. Q.; Kirlikovali, K. O.; Suh, J. M.; Choi, J. W.; Jang, H. W.; Varma, R. S.; Farha, O. K.; Shokouhimehr, M. Recent Advances in Rechargeable Aluminum-Ion Batteries and Considerations for Their Future Progress. *Acs Applied Energy Materials* **2020**, *3* (7), 6019-6035, DOI: 10.1021/acsaem.0c00957.
- (9) Huang, J. H.; Guo, Z. W.; Ma, Y. Y.; Bin, D.; Wang, Y. G.; Xia, Y. Y. Recent Progress of Rechargeable Batteries Using Mild Aqueous Electrolytes. *Small Methods* **2019**, *3* (1), DOI: 10.1002/smt.201800272.

- (10) Hudak, N. S. Chloroaluminate-Doped Conducting Polymers as Positive Electrodes in Rechargeable Aluminum Batteries. *Journal of Physical Chemistry C* **2014**, *118* (10), 5203-5215, DOI: 10.1021/jp500593d.
- (11) Wang, C. L. Weak Intermolecular Interactions for Strengthening Organic Batteries. *Energy & Environmental Materials* **2020**, *3* (4), 441-452, DOI: 10.1002/eem2.12076.
- (12) Xu, S. F.; Sun, M. X.; Wang, Q.; Wang, C. L. Recent progress in organic electrodes for zinc-ion batteries. *Journal of Semiconductors* **2020**, *41* (9), DOI: 10.1088/1674-4926/41/9/091704.
- (13) Wan, F.; Zhang, L. L.; Wang, X. Y.; Bi, S. S.; Niu, Z. Q.; Chen, J. An Aqueous Rechargeable Zinc-Organic Battery with Hybrid Mechanism. *Advanced Functional Materials* **2018**, *28* (45), DOI: 10.1002/adfm.201804975.
- (14) Li, X. W.; Xie, X. L.; Lv, R. H.; Na, B.; Wang, B.; He, Y. Nanostructured Polypyrrole Composite Aerogels for a Rechargeable Flexible Aqueous Zn-Ion Battery with High Rate Capabilities. *Energy Technology* **2019**, *7* (5), 6, DOI: 10.1002/ente.201801092.
- (15) Liu, Y.; Xie, L. Y.; Zhang, W.; Dai, Z. W.; Wei, W.; Luo, S. J.; Chen, X.; Chen, W.; Rao, F.; Wang, L.; Huang, Y. Conjugated System of PEDOT:PSS-Induced Self-Doped PANI for Flexible Zinc-Ion Batteries with Enhanced Capacity and Cyclability. *Acs Applied Materials & Interfaces* **2019**, *11* (34), 30943-30952, DOI: 10.1021/acsami.9b09802.
- (16) Chen, Y.; Zhuo, S. M.; Li, Z. Y.; Wang, C. L. Redox polymers for rechargeable metal-ion batteries. *Energychem* **2020**, *2* (2), DOI: 10.1016/j.enchem.2020.100030.
- (17) Pickup, P. G.; Osteryoung, R. A. Charging and discharging rate studies of polypyrrole films in AlCl_3 -1-methyl-(3-ethyl)-imidazolium chloride molten-salts and in CH_3CN . *Journal of Electroanalytical Chemistry* **1985**, *195* (2), 271-288, DOI: 10.1016/0022-0728(85)80048-6.
- (18) Janiszewska, L.; Osteryoung, R. A. Electrochemistry of polythiophene and polybithiophene films in ambient-temperature molten-salts. *Journal of the Electrochemical Society* **1987**, *134* (11), 2787-2794, DOI: 10.1149/1.2100288.
- (19) Takeishi, K.; Koura, N.; Ito, S. Application of a polyaniline polyanion composite film to a positive electrode for an aluminum secondary cell with an ambient-temperature molten-salt electrolyte. *Denki Kagaku* **1995**, *63* (7), 629-633.
- (20) Goldenberg, L. M.; Osteryoung, R. A. Benzene polymerization in 1-ethyl-3-methylimidazolium chloride AlCl_3 ionic liquid. *Synthetic Metals* **1994**, *64* (1), 63-68, DOI: 10.1016/0379-6779(94)90276-3.
- (21) Vujkovic, M. J.; Etinski, M.; Vasic, B.; Kuzmanovic, B.; Bajuk-Bogdanovic, D.; Dominko, R.; Mentus, S. Polyaniline as a charge storage material in an aqueous aluminum-based electrolyte: Can aluminum ions play the role of protons? *J. Power Sources* **2021**, *482*, DOI: 10.1016/j.jpowsour.2020.228937.
- (22) El Rhazi, M.; Majid, S. Electrochemical sensors based on polydiaminonaphthalene and polyphenylenediamine for monitoring metal pollutants. *Trends in Environmental Analytical Chemistry* **2014**, *2*, 33-42, DOI: 10.1016/j.teac.2014.02.001.
- (23) Li, X. G.; Huang, M. R.; Duan, W.; Yang, Y. L. Novel multifunctional polymers from aromatic diamines by oxidative polymerizations. *Chemical Reviews* **2002**, *102* (9), 2925-3030, DOI: 10.1021/cr010423z.
- (24) Wang, L.; Zhu, H. Z.; Song, Y. H.; Liu, L.; He, Z. F.; Wan, L. L.; Chen, S. H.; Xiang, Y.; Chen, S. S.; Chen, J. Architecture of poly(o-phenylenediamine)-Ag nanoparticle composites for a hydrogen peroxide sensor. *Electrochimica Acta* **2012**, *60*, 314-320, DOI: 10.1016/j.electacta.2011.11.045.
- (25) Yuan, C. Q.; Liu, X. H.; Jia, M. Y.; Luo, Z. X.; Yao, J. N. Facile preparation of N- and O-doped hollow carbon spheres derived from poly(o-phenylenediamine) for supercapacitors. *J. Mater. Chem. A* **2015**, *3* (7), 3409-3415, DOI: 10.1039/c4ta06411a.
- (26) Xu, L. H.; Sun, Y.; Han, B.; Su, C. Electrochemical Performances on Both poly(Phenylenediamine) Derivatives as Anode of Lithium-Ion Batteries. *Journal of the Electrochemical Society* **2019**, *166* (8), A1363-A1369, DOI: 10.1149/2.0351908jes.
- (27) Sivakkumar, S. R.; Sivakkumar, S. R. Application of poly(o-phenylenediamine) in rechargeable cells. *Journal of Applied Electrochemistry* **2004**, *34* (11), 1147-1152, DOI: 10.1007/s10800-004-3302-8.

- (28) Zhang, S. Q.; Long, S. T.; Li, H.; Xu, Q. A high-capacity organic cathode based on active N atoms for aqueous zinc-ion batteries. *Chemical Engineering Journal* **2020**, *400*, DOI: 10.1016/j.cej.2020.125898.
- (29) Shpigel, N.; Levi, M. D.; Aurbach, D. EQCM-D technique for complex mechanical characterization of energy storage electrodes: Background and practical guide. *Energy Storage Materials* **2019**, *21*, 399-413, DOI: 10.1016/j.ensm.2019.05.026.
- (30) Shpigel, N.; Levi, M. D.; Sigalov, S.; Daikhin, L.; Aurbach, D. In Situ Real-Time Mechanical and Morphological Characterization of Electrodes for Electrochemical Energy Storage and Conversion by Electrochemical Quartz Crystal Microbalance with Dissipation Monitoring. *Accounts of Chemical Research* **2018**, *51* (1), 69-79, DOI: 10.1021/acs.accounts.7b00477.
- (31) Hillman, A. R. The Electrochemical Quartz Crystal Microbalance. In *Encyclopedia of Electrochemistry* **2007**, DOI: 10.1002/9783527610426.bard030207.
- (32) Kitz, P. G.; Lacey, M. J.; Novak, P.; Berg, E. J. Operando EQCM-D with Simultaneous in Situ EIS: New Insights into Interphase Formation in Li Ion Batteries. *Analytical Chemistry* **2019**, *91* (3), 2296-2303, DOI: 10.1021/acs.analchem.8b04924.
- (33) Lemaire, P.; Dargon, T.; Dalla Corte, D. A.; Sel, O.; Perrot, H.; Tarascon, J. M. Making Advanced Electrogravimetry as an Affordable Analytical Tool for Battery Interface Characterization. *Analytical Chemistry* **2020**, *92* (20), 13803-13812, DOI: 10.1021/acs.analchem.0c02233.
- (34) Levi, M. D.; Salitra, G.; Levy, N.; Aurbach, D.; Maier, J. Application of a quartz-crystal microbalance to measure ionic fluxes in microporous carbons for energy storage. *Nature Materials* **2009**, *8* (11), 872-875, DOI: 10.1038/nmat2559.
- (35) Srimuk, P.; Lee, J.; Budak, O.; Choi, J.; Chen, M.; Feng, G.; Prehal, C.; Presser, V. In Situ Tracking of Partial Sodium Desolvation of Materials with Capacitive, Pseudocapacitive, and Battery-like Charge/Discharge Behavior in Aqueous Electrolytes. *Langmuir* **2018**, *34* (44), 13132-13143, DOI: 10.1021/acs.langmuir.8b02485.
- (36) Tsai, W. Y.; Taberna, P. L.; Simon, P. Electrochemical Quartz Crystal Microbalance (EQCM) Study of Ion Dynamics in Nanoporous Carbons. *Journal of the American Chemical Society* **2014**, *136* (24), 8722-8728, DOI: 10.1021/ja503449w.
- (37) Levi, M. D.; Shpigel, N.; Sigalov, S.; Dargel, V.; Daikhin, L.; Aurbach, D. In Situ Porous Structure Characterization of Electrodes for Energy Storage and Conversion by EQCM-D: a Review. *Electrochimica Acta* **2017**, *232*, 271-284, DOI: 10.1016/j.electacta.2017.02.149.
- (38) Shpige, N.; Sigalov, S.; Levi, M. D.; Mathis, T.; Daikhin, L.; Janes, A.; Lust, E.; Gogotsi, Y.; Aurbach, D. In Situ Acoustic Diagnostics of Particle-Binder Interactions in Battery Electrodes. *Joule* **2018**, *2* (5), 988-1003, DOI: 10.1016/j.joule.2018.02.014.
- (39) Halim, E.; Demir-Cakan, R.; Debiemme-Chouvy, C.; Perrot, H.; El Rhazi, M.; Sel, O. Poly(ortho-phenylenediamine) overlaid fibrous carbon networks exhibiting a synergistic effect for enhanced performance in hybrid micro energy storage devices. *J. Mater. Chem. A* **2021**, *9* (16), 10487-10496, DOI: 10.1039/d1ta00763g.
- (40) Halim, E.; Demir-Cakan, R.; Perrot, H.; El Rhazi, M.; Sel, O. Correlation between the interfacial ion dynamics and charge storage properties of poly(ortho-phenylenediamine) electrodes exhibiting high cycling stability. *Journal of Power Sources* **2019**, *438*, DOI: 10.1016/j.jpowsour.2019.227032.
- (41) Sauerbrey, G. Verwendung von schwingquarzen zur wagung dunner schichten und zur mikrowagung. *Zeitschrift Fur Physik* **1959**, *155* (2), 206-222, DOI: 10.1007/bf01337937.
- (42) Muthirulan, P.; Rajendran, N. Poly(o-phenylenediamine) coatings on mild steel: Electrosynthesis, characterization and its corrosion protection ability in acid medium. *Surface & Coatings Technology* **2012**, *206* (8-9), 2072-2078, DOI: 10.1016/j.surfcoat.2011.09.008.
- (43) Malinauskas, A.; Bron, M.; Holze, R. Electrochemical and Raman spectroscopic studies of electrosynthesized copolymers and bilayer structures of polyaniline and poly(o-phenylenediamine). *Synthetic Metals* **1998**, *92* (2), 127-137, DOI: 10.1016/s0379-6779(98)80102-1.
- (44) Yano, J. Electrochemical and structural studies on soluble and conducting polymer from o-phenylenediamine. *Journal of Polymer Science Part a-Polymer Chemistry* **1995**, *33* (14), 2435-2441, DOI: 10.1002/pola.1995.080331416.

- (45) Wang, M. R.; Zhang, H. H.; Wang, C. Y.; Hu, X. Y.; Wang, G. X. Direct electrosynthesis of poly(o-phenylenediamine) bulk materials for supercapacitor application. *Electrochimica Acta* **2013**, *91*, 144-151, DOI: 10.1016/j.electacta.2012.12.087.
- (46) Zhang, X. H.; Wang, S. M.; Wu, J.; Liu, X. J. Electropolymerization of PoPD from aqueous solutions of sodium dodecyl benzene sulfonate at conducting glass electrode. *Journal of Applied Polymer Science* **2007**, *104* (3), 1928-1932, DOI: 10.1002/app.25877.
- (47) Pullicino, E.; Zou, W. T.; Gresil, M.; Soutis, C. The Effect of Shear Mixing Speed and Time on the Mechanical Properties of GNP/Epoxy Composites. *Applied Composite Materials* **2017**, *24* (2), 301-311, DOI: 10.1007/s10443-016-9559-3.
- (48) Chiba, K.; Ohsaka, T.; Ohnuki, Y.; Oyama, N. Electrochemical preparation of a ladder polymer containing phenazine rings. *Journal of Electroanalytical Chemistry* **1987**, *219* (1-2), 117-124, DOI: 10.1016/0022-0728(87)85034-9.
- (49) Ogura, K.; Shiigi, H.; Nakayama, M. A new humidity sensor using the composite film derived from poly(o-phenylenediamine) and poly(vinyl alcohol). *Journal of the Electrochemical Society* **1996**, *143* (9), 2925-2930, DOI: 10.1149/1.1837128.
- (50) Zhang, Q. L.; Lin, N.; Xu, T. J.; Shen, K. Z.; Li, T. Q.; Han, Y.; Zhou, J.; Qian, Y. T. Scalable synthesis of carbon stabilized SiO/graphite sheets composite as anode for high-performance Li ion batteries. *Rsc Advances* **2017**, *7* (63), 39762-39766, DOI: 10.1039/c7ra05829b.
- (51) Ullah, H.; Shah, A. U. A.; Ayub, K.; Bilal, S. Density Functional Theory Study of Poly(o-phenylenediamine) Oligomers. *Journal of Physical Chemistry C* **2013**, *117* (8), 4069-4078, DOI: 10.1021/jp311526u.
- (52) Samanta, S.; Roy, P.; Kar, P. Structure and properties of conducting poly(o-phenylenediamine) synthesized in different inorganic acid medium. *Macromolecular Research* **2016**, *24* (4), 342-349, DOI: 10.1007/s13233-016-4054-0.
- (53) Peacock, J. C.; Peacock, B. L. D. Some observations the dissolving of zinc chloride and several suggested solvents. *The Journal of the American Pharmaceutical Association* **1918**, *7* (8), 689-697, DOI: doi.org/10.1002/jps.3080070807
- (54) Zhao, Q.; Zachman, M. J.; Al Sadat, W. I.; Zheng, J. X.; Kourkoutis, L. F.; Archer, L. Solid electrolyte interphases for high-energy aqueous aluminum electrochemical cells. *Science Advances* **2018**, *4* (11), DOI: 10.1126/sciadv.aau8131.
- (55) Zuo, W. H.; Zhu, W. H.; Zhao, D. F.; Sun, Y. F.; Li, Y. Y.; Liu, J. P.; Lou, X. W. Bismuth oxide: a versatile high-capacity electrode material for rechargeable aqueous metal-ion batteries. *Energy & Environmental Science* **2016**, *9* (9), 2881-2891, DOI: 10.1039/c6ee01871h.
- (56) Wu, X. B.; Qin, N.; Wang, F.; Li, Z. H.; Qin, J. Y.; Huang, G. J.; Wang, D. H.; Liu, P.; Yao, Q. R.; Lu, Z. G.; Deng, J. Q. Reversible aluminum ion storage mechanism in Ti-deficient rutile titanium dioxide anode for aqueous aluminum-ion batteries. *Energy Storage Materials* **2021**, *37*, 619-627, DOI: 10.1016/j.ensm.2021.02.040.
- (57) Tie, Z. W.; Liu, L. J.; Deng, S. Z.; Zhao, D. B.; Niu, Z. Q. Proton Insertion Chemistry of a Zinc-Organic Battery. *Angewandte Chemie-International Edition* **2020**, *59* (12), 4920-4924, DOI: 10.1002/anie.201916529.
- (58) Emanuelsson, R.; Sterby, M.; Stromme, M.; Sjodin, M. An All-Organic Proton Battery. *Journal of the American Chemical Society* **2017**, *139* (13), 4828-4834, DOI: 10.1021/jacs.7b00159.
- (59) Li, K. R.; Shao, Y. L.; Liu, S. Y.; Zhang, Q. H.; Wang, H. Z.; Li, Y. G.; Kaner, R. B. Aluminum-Ion-Intercalation Supercapacitors with Ultrahigh Areal Capacitance and Highly Enhanced Cycling Stability: Power Supply for Flexible Electrochromic Devices. *Small* **2017**, *13* (19), DOI: 10.1002/sml.201700380.
- (60) Swaddle, T. W.; Rosenqvist, J.; Yu, P.; Bylaska, E.; Phillips, B. L.; Casey, W. H. Kinetic evidence for five-coordination in $\text{AlOH(aq)}(2+)$ ion. *Science* **2005**, *308* (5727), 1450-1453, DOI: 10.1126/science.1110231.
- (61) Yang, W. H.; Du, X. F.; Zhao, J. W.; Chen, Z.; Li, J. J.; Xie, J.; Zhang, Y. J.; Cui, Z. L.; Kong, Q. Y.; Zhao, Z. M.; Wang, C. G.; Zhang, Q. C.; Cui, G. L. Hydrated Eutectic Electrolytes with Ligand-Oriented Solvation

- Shells for Long-Cycling Zinc-Organic Batteries. *Joule* **2020**, 4 (7), 1557-1574, DOI: 10.1016/j.joule.2020.05.018.
- (62) Wang, J.; Polleux, J.; Lim, J.; Dunn, B. Pseudocapacitive contributions to electrochemical energy storage in TiO₂ (anatase) nanoparticles. *Journal of Physical Chemistry C* **2007**, 111 (40), 14925-14931, DOI: 10.1021/jp074464w.
- (63) Tan, Y.; An, F. Q.; Liu, Y. C.; Li, S. W.; He, P. G.; Zhang, N.; Li, P.; Qu, X. H. Reaction kinetics in rechargeable zinc-ion batteries. *Journal of Power Sources* **2021**, 492, DOI: 10.1016/j.jpowsour.2021.229655.
- (64) Thalji, M. R.; Ali, G. A. M.; Liu, P. R.; Zhong, Y. L.; Chong, K. F. W18O₄₉ nanowires-graphene nanocomposite for asymmetric supercapacitors employing AlCl₃ aqueous electrolyte. *Chemical Engineering Journal* **2021**, 409, DOI: 10.1016/j.cej.2020.128216.
- (65) Gao, W. L.; Krins, N.; Laberty-Robert, C.; Perrot, H.; Sel, O. Scrutiny of the LiCoO₂ Composite Electrode/Electrolyte Interface by Advanced Electrogravimetry and Implications for Aqueous Li-Ion Batteries. *Journal of Physical Chemistry C* **2021**, 125 (7), 3859-3867, DOI: 10.1021/acs.jpcc.0c09708.
- (66) Shao, H.; Xu, K.; Wu, Y. C.; Iadecola, A.; Liu, L. Y.; Ma, H. Y.; Qu, L. T.; Raymundo-Pinero, E.; Zhu, J. X.; Lin, Z. F.; Taberna, P. L.; Simon, P. Unraveling the Charge Storage Mechanism of Ti₃C₂TX MXene Electrode in Acidic Electrolyte. *Acs Energy Letters* **2020**, 5 (9), 2873-2880, DOI: 10.1021/acsenenergylett.0c01290.
- (67) Gupta, T.; Kim, A.; Phadke, S.; Biswas, S.; Luong, T.; Hertzberg, B. J.; Chamoun, M.; Evans-Lutterodt, K.; Steingart, D. A. Improving the cycle life of a high-rate, high-potential aqueous dual ion battery using hyper-dendritic zinc and copper hexacyanoferrate. *Journal of Power Sources* **2016**, 305, 22-29, DOI: 10.1016/j.jpowsour.2015.11.065.
- (68) Huang, S.; Zhu, J. C.; Tian, J. L.; Niu, Z. Q. Recent Progress in the Electrolytes of Aqueous Zinc-Ion Batteries. *Chemistry-a European Journal* **2019**, 25 (64), 14480-14494, DOI: 10.1002/chem.201902660.
- (69) Kundu, D.; Vajargah, S. H.; Wan, L. W.; Adams, B.; Prendergast, D.; Nazar, L. F. Aqueous vs. nonaqueous Zn-ion batteries: consequences of the desolvation penalty at the interface. *Energy & Environmental Science* **2018**, 11 (4), 881-892, DOI: 10.1039/c8ee00378e.
- (70) Lee, B.; Lee, H. R.; Kim, H.; Chung, K. Y.; Cho, B. W.; Oh, S. H. Elucidating the intercalation mechanism of zinc ions into alpha-MnO₂ for rechargeable zinc batteries. *Chem. Commun.* **2015**, 51 (45), 9265-9268, DOI: 10.1039/c5cc02585k.
- (71) Pan, H. L.; Shao, Y. Y.; Yan, P. F.; Cheng, Y. W.; Han, K. S.; Nie, Z. M.; Wang, C. M.; Yang, J. H.; Li, X. L.; Bhattacharya, P.; Mueller, K. T.; Liu, J. Reversible aqueous zinc/manganese oxide energy storage from conversion reactions. *Nature Energy* **2016**, 1, DOI: 10.1038/nenergy.2016.39.
- (72) Liu, L. Y.; Wu, Y. C.; Huang, L.; Liu, K. S.; Duployer, B.; Rozier, P.; Taberna, P. L.; Simon, P. Alkali Ions Pre-Intercalated Layered MnO₂ Nanosheet for Zinc-Ions Storage. *Advanced Energy Materials* **2021**, 11 (31), DOI: 10.1002/aenm.202101287.
- (73) Lin, Z. R.; Shi, H. Y.; Lin, L.; Yang, X. P.; Wu, W. L.; Sun, X. Q. A high capacity small molecule quinone cathode for rechargeable aqueous zinc-organic batteries. *Nature Communications* **2021**, 12 (1), DOI: 10.1038/s41467-021-24701-9.
- (74) Gavriel, B.; Shpigel, N.; Malchik, F.; Bergman, G.; Turgeman, M.; Levi, M. D.; Aurbach, D. Enhanced Performance of Ti₃C₂Tx (MXene) Electrodes in Concentrated ZnCl₂ Solutions: A Combined Electrochemical and EQCM-D Study. *Energy Storage Materials* **2021**, 38, 535-541, DOI: 10.1016/j.ensm.2021.03.027.
- (75) Balland, V.; Mateos, M.; Singh, A.; Harris, K. D.; Laberty-Robert, C.; Limoges, B. The Role of Al³⁺-Based Aqueous Electrolytes in the Charge Storage Mechanism of MnO_x Cathodes. *Small* **2021**, 17 (23), DOI: 10.1002/smll.202101515.
- (76) Zhao, Q.; Liu, L. J.; Yin, J. F.; Zheng, J. X.; Zhang, D. H.; Chen, J.; Archer, L. A. Proton Intercalation/De-Intercalation Dynamics in Vanadium Oxides for Aqueous Aluminum Electrochemical Cells. *Angewandte Chemie-International Edition* **2020**, 59 (8), 3048-3052, DOI: 10.1002/anie.201912634.

(77) Lee, B.; Seo, H. R.; Lee, H. R.; Yoon, C. S.; Kim, J. H.; Chung, K. Y.; Cho, B. W.; Oh, S. H. Critical Role of pH Evolution of Electrolyte in the Reaction Mechanism for Rechargeable Zinc Batteries. *Chemsuschem* **2016**, 9 (20), 2948-2956, DOI: 10.1002/cssc.201600702.

TOC graphic for

Aqueous Multivalent Charge Storage Mechanism in Aromatic Diamine Based Organic Electrodes

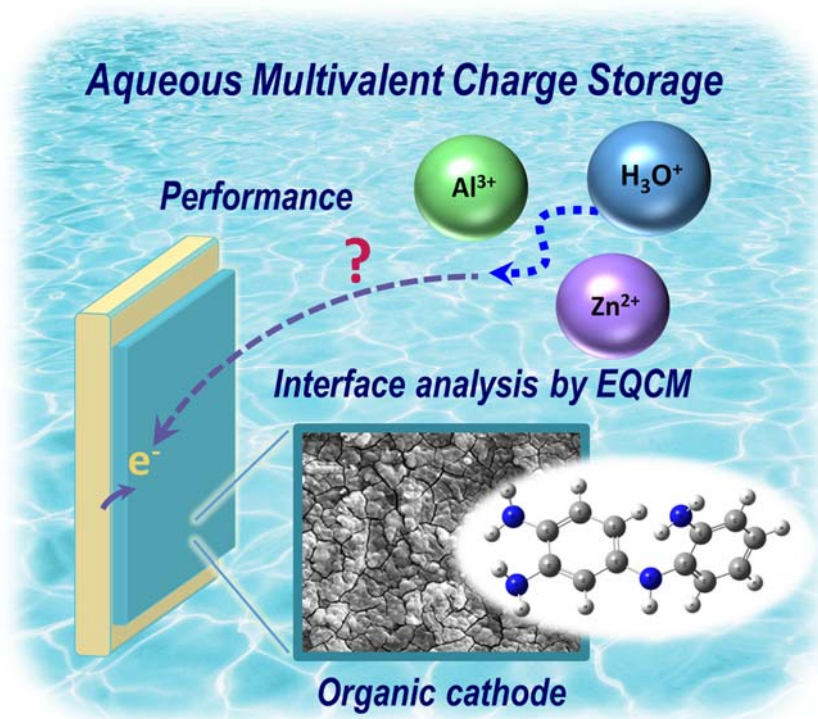
Selin Sariyer^a, Arpita Ghosh^b, Sevde Nazli Dambasan^a, El Mahdi Halim^{b,c}, Mama El Rhazfi, Hubert

Perrot^b, Ozlem Sel^{b,*} and Rezan Demir-Cakan^{a,*}

^a Gebze Technical University, Department of Chemical Engineering, 41400 Gebze, Kocaeli, Turkey

^b Sorbonne Université, CNRS, Laboratoire Interfaces et Systèmes Electrochimiques, LISE, 75005 Paris, France

^c University of Hassan II of Casablanca, Faculty of Sciences and Technology, Laboratory of Materials, Membranes and Environment -BP 146, 20650 Mohammedia, Morocco



SUPPORTING INFORMATION FOR

Aqueous Multivalent Charge Storage Mechanism in Aromatic Diamine Based Organic Electrodes

Selin Sariyer^a, Arpita Ghosh^b, Sevde Nazli Dambasan^a, El Mahdi Halim^{b,c}, Mama El Rhazfi, Hubert

Perrot^b, Ozlem Sel^{b,*} and Rezan Demir-Cakan^{a,*}

^a Gebze Technical University, Department of Chemical Engineering, 41400 Gebze, Kocaeli, Turkey

^b Sorbonne Université, CNRS, Laboratoire Interfaces et Systèmes Electrochimiques, LISE, 75005 Paris, France

^c University of Hassan II of Casablanca, Faculty of Sciences and Technology, Laboratory of Materials, Membranes and Environment -BP 146, 20650 Mohammedia, Morocco

TABLE OF CONTENTS

Part A. FTIR spectrum.....SI-2

Figure S1. FTIR spectrum of the graphite substrate.

Part B. Rationalization of the molecular structure of PoPD repeating unit by DFT method.....SI-3

Figure S2. (a) Phenazine-like structure of PoPD (b) 1,4-substituted benzenoid-quinoid structure of PoPD.

Part C. The structural stability of the PoPD electrodes after long-term cycling process.....SI-3

Figure S3. SEM images of (a) PoPD electrode, after long term cycling process (b) in 1 M ZnSO₄ electrolyte, (c) in 0.25 M AlCl₃ electrolyte.

Part D. Experiments on the role of proton for the CE values.....SI-4

Figure S4. (a) Discharge charge curves of PoPD electrode in 0.25 M AlCl₃ + 0.03 M HCl electrolyte (b) cycling performances at a current density of 5C in both 0.25 M AlCl₃ and in 0.25 M AlCl₃ + 0.03 M HCl electrolytes

Part E. The contribution of the capacitive and diffusion-controlled process calculations.....SI-4

Figure S5, S6. The contribution of the capacitive and diffusion-controlled process calculations: the plot of log(i) vs. log(ν) of the PoPD electrodes.

Part F. Diffusion coefficient estimation by Electrochemical Impedance Spectroscopy.....SI-5

Figures S7, S8, S9. Diffusion coefficient estimation by Electrochemical Impedance Spectroscopy.

Part G. EQCM with motional resistance monitoring of PoPD.....SI-8

Figures S10, S11. EQCM with motional resistance monitoring of PoPD.

Scheme S1: Schematic description of dissimilar behavior of PoPD in the different electrolytes.

Part H. EDS spectrum of the cycled PoPD electrodes.....SI-9

Figure S12. EDS spectrum of the cycled PoPD electrodes.

Part I. Literature comparisons.....SI-10

Table S1: Organic cathode materials in aqueous electrolyte Zn-ion batteries

Table S2: Organic cathode materials in aqueous electrolyte Al-ion batteries

References.....SI-12

Part A. FTIR spectrum

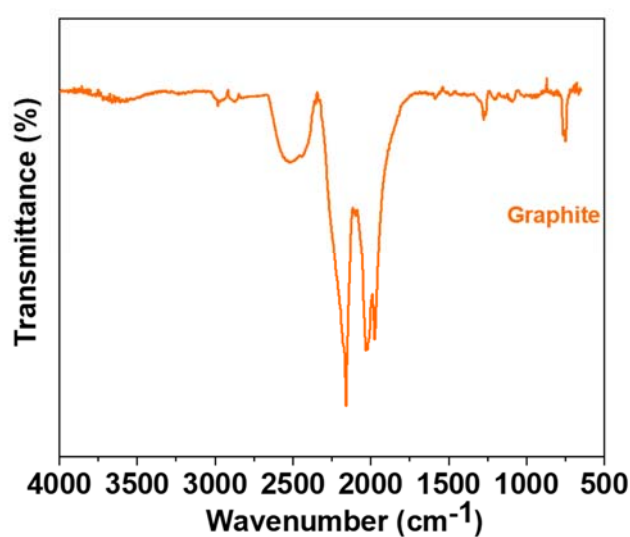


Figure S1. FTIR spectrum of the graphite substrate used in this study.

Part B. Rationalization of the molecular structure of PoPD repeating unit by DFT method

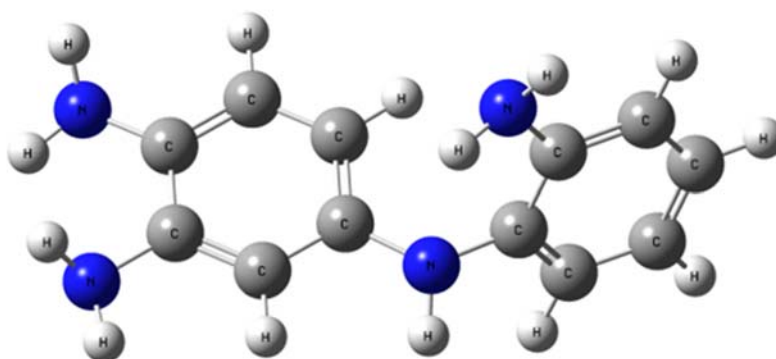


Figure S2. 1,4-substituted benzenoid-quinoid structure of PoPD. Note: blue is N, dark gray is C and light gray is H atoms.

Part C. The structural stability of the PoPD electrodes after long-term cycling process

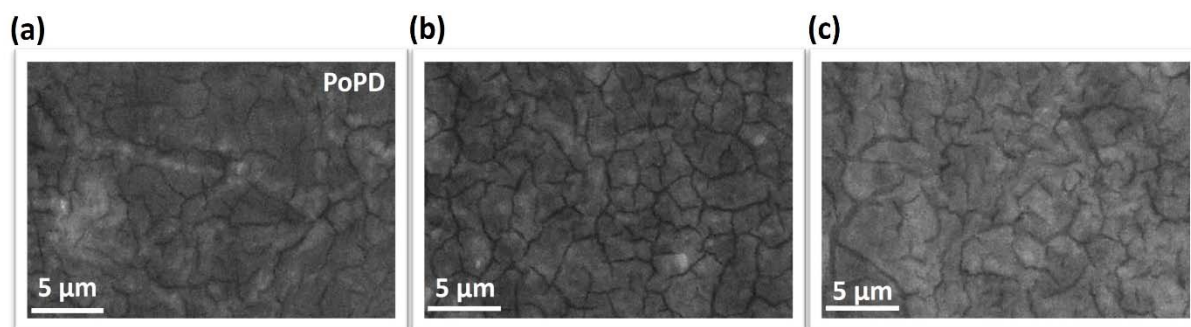


Figure S3. SEM images of (a) PoPD electrode, after long term cycling process (b) in 1 M ZnSO_4 electrolyte, (c) in 0.25 M AlCl_3 electrolyte.

Part D. Experiments on the role of proton for the CE values

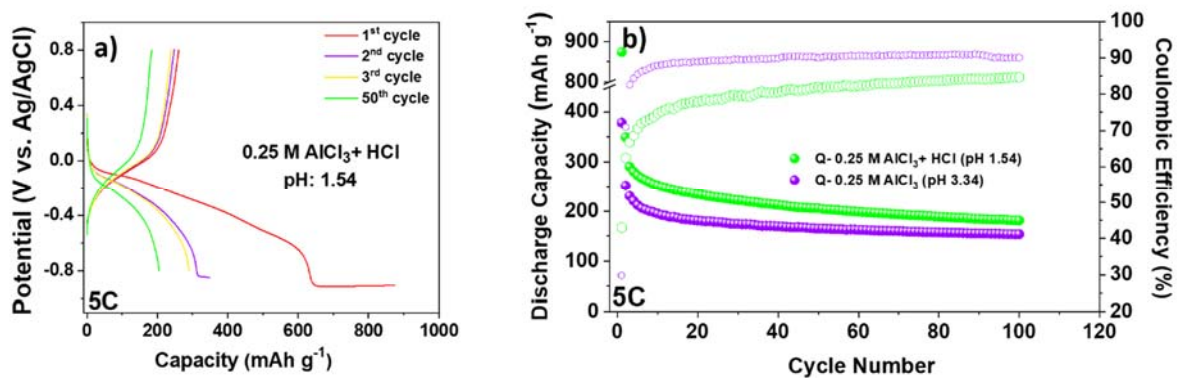


Figure S4. (a) Discharge charge curves of PoPD electrode in 0.25 M AlCl_3 + 0.03 M HCl electrolyte (b) cycling performances at a current density of 5C in both 0.25 M AlCl_3 and in 0.25 M AlCl_3 + 0.03 M HCl electrolytes.

E. The contribution of the capacitive and diffusion-controlled process calculations: the plot of $\log(i)$ vs. $\log(v)$ of the PoPD electrodes

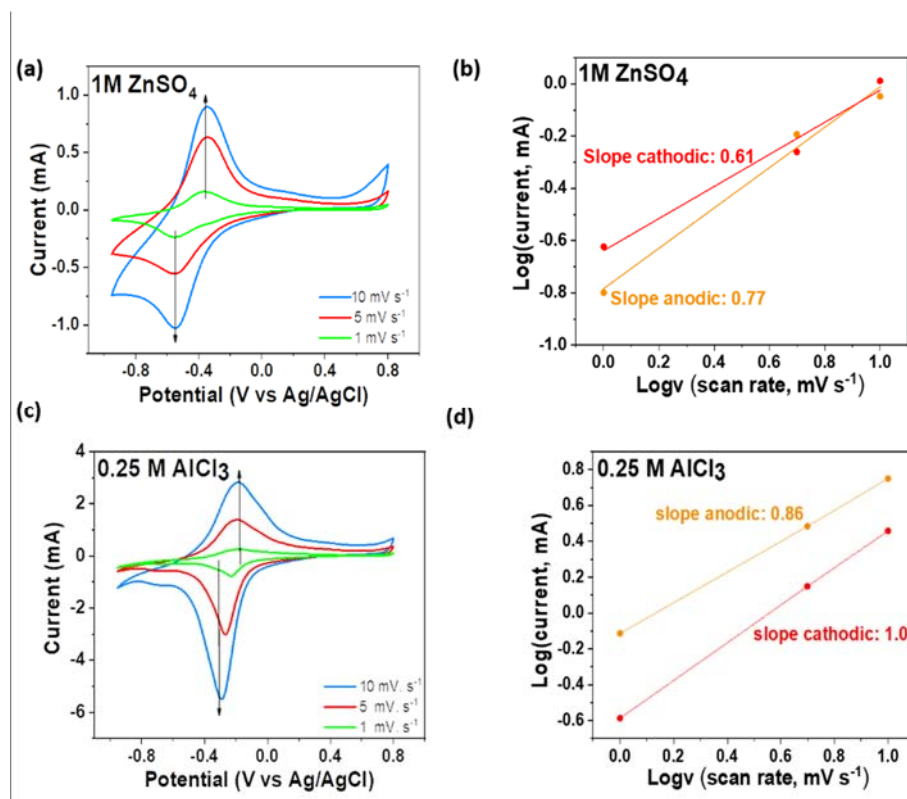


Figure S5: PoPD electrode in 1 M ZnSO₄ electrolyte, (a) CV curves at 1, 5 and 10 mV s⁻¹ scan rates, (b) the plot of $\log(i)$ vs. $\log(v)$. PoPD electrode in 0.25 M AlCl₃ electrolyte, (c) CV curves at 1, 5 and 10 mV s⁻¹ scan rates, (d) the plot of $\log(i)$ vs. $\log(v)$.

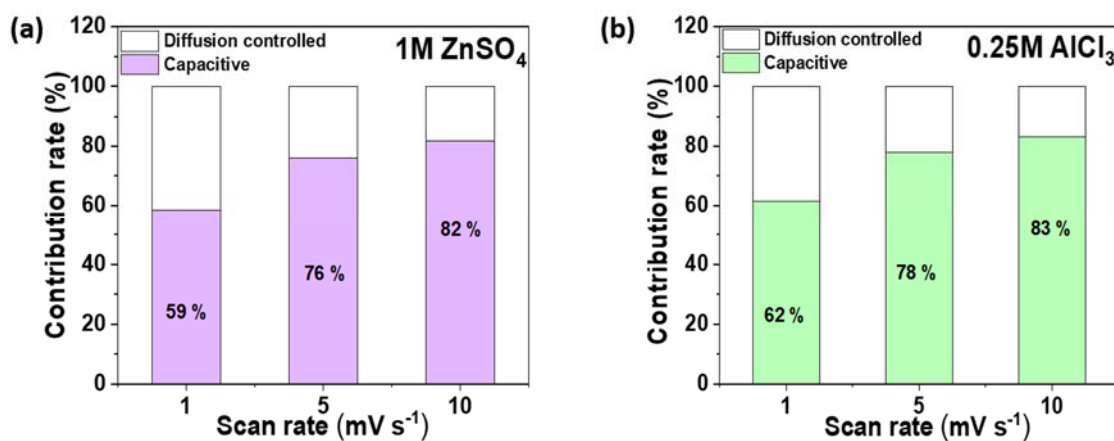


Figure S6: Capacitive and diffusion-controlled contribution at different scan rates of the PoPD electrode on graphite (a) in 1 M ZnSO₄, (b) in 0.25 M AlCl₃.

The faradaic, pseudo-capacitance and non-faradaic contribution can be scrutinized by analyzing CV recorded at various scan rates. In Equation S1, i and v represent the currents values and scan rates, respectively.

$$i = av^b \quad (\text{Equation S1})$$

In this equation, a and b are constants in which b values were determined from the slope of $\log(i)$ (mA) vs. $\log(v)$ (mV s⁻¹) and found 0.61 for anodic and 0.77 for cathodic processes in 1 M ZnSO₄ (Figure S5-b). Likewise, the b -values of oxidation and reduction from the slope of $\log(i)$ vs. $\log(v)$ plot (Figure S5-d) in 0.25 M AlCl₃ were calculated as 0.86 and 1.0, respectively. It was described that when b is near to 1, the capacitive process is dominant in the charge storage mechanism; however, if the b value is 0.5, diffusion of ionic species (in Al³⁺ or Zn²⁺ containing electrolytes) mainly control the electrochemical process. Thus, higher b values for PoPD electrode than 0.5 state that electrochemical reaction is controlled by a capacitive process (surface-controlled). Then, the contribution of the capacitive and diffusion controlled process was estimated and demonstrated in Figure S6.

F. Diffusion coefficient estimation by Electrochemical Impedance Spectroscopy

$$D = \frac{R^2 T^2}{2A^2 n^4 F^4 C^2 \sigma^2} \quad (\text{Equation S2})$$

where R , C , T , A , n , F , and σ represent gas constant (8.314 J mol⁻¹ K⁻¹), concentration of ions, absolute temperature (298.15 K), surface area of PoPD (2 cm²), electrons transferred, Faraday constant (96500 C mol⁻¹), and Warburg coefficient, respectively. Furthermore, Warburg coefficient can be predicted according to the following expression:

$$Z' = R_s + R_{ct} + \sigma \omega^{-1/2} \quad (\text{Equation S3})$$

where Z' , R_s , R_{ct} and ω indicate value of impedance, resistance between host material and electrolytes, charge transfer resistance and angular frequency, respectively.

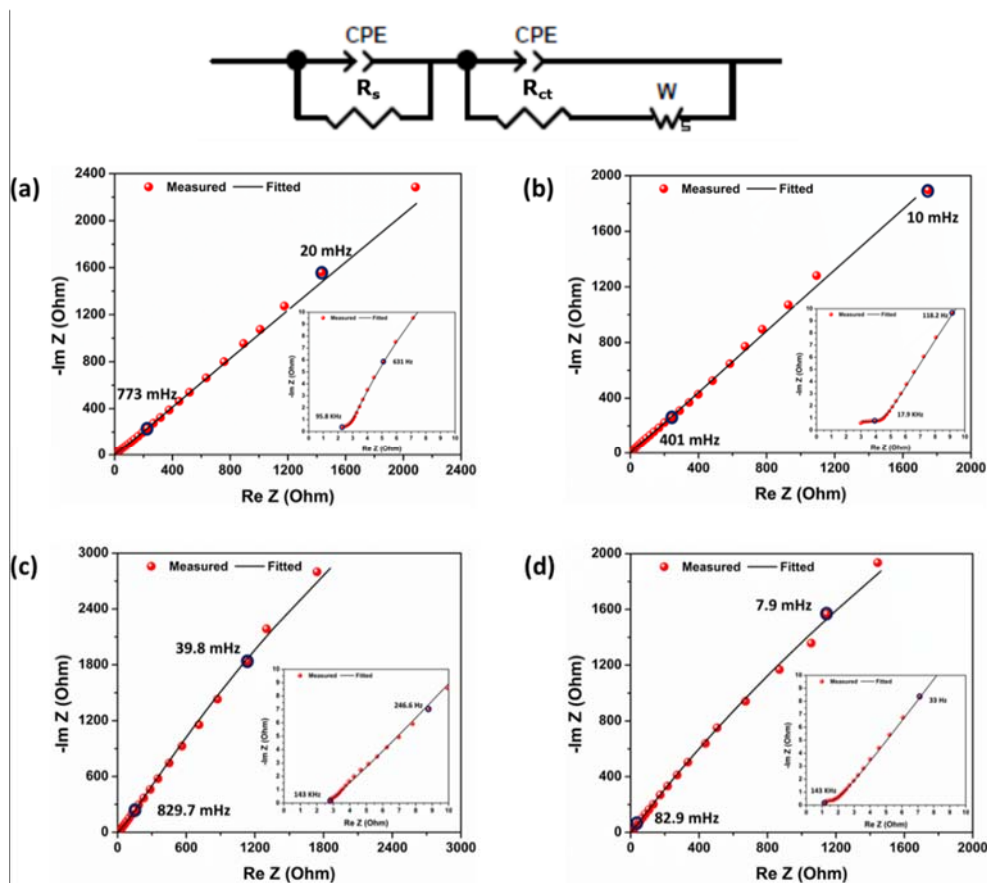


Figure S7: Nyquist plot along with the equivalent circuit (top) of PoPD electrode in 1 M ZnSO_4 electrolyte measured at initial (a) and final (b) C-rate and in 0.25 M AlCl_3 electrolyte measured at initial (c) and final (d) C-rate.

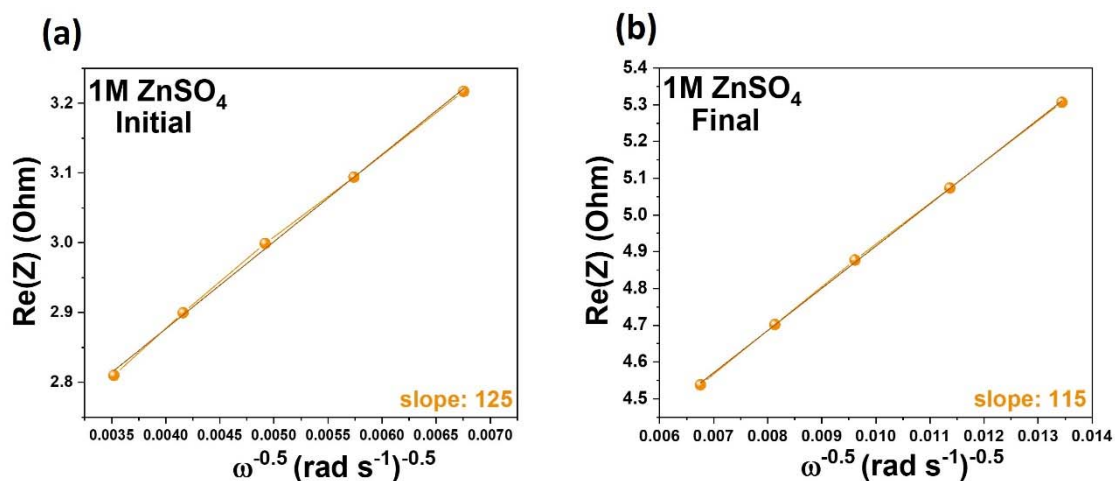


Figure S8: The plot of Z' vs. $\omega^{-0.5}$ in the low frequency range of PoPD film electrode in 1 M ZnSO_4 (a) initial C-rate (b) final C-rate.

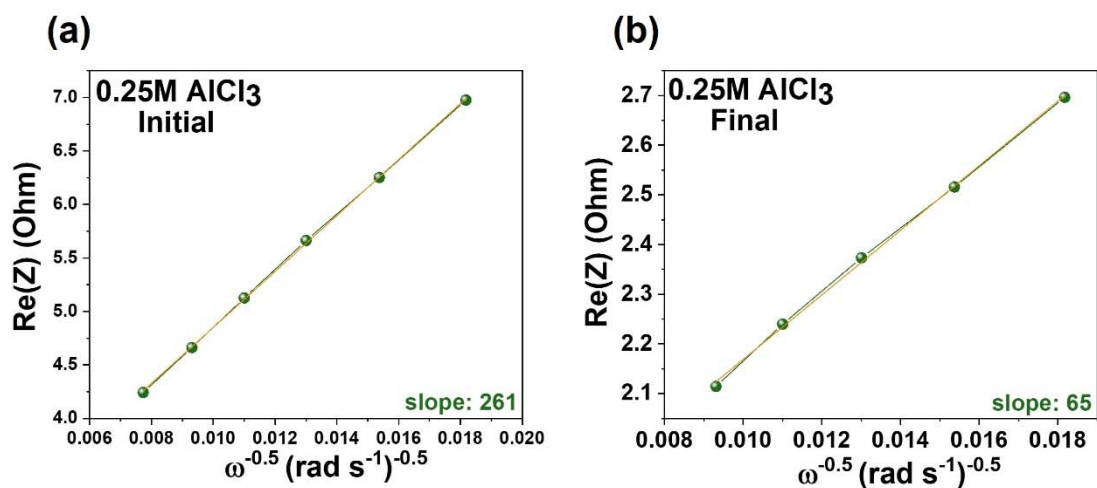


Figure S9: The plot of Z' vs. $\omega^{-0.5}$ in the low frequency range of PoPD film electrode in 0.25 M AlCl₃ (a) initial C-rate (b) final C-rate.

G. EQCM with motional resistance monitoring of PoPD

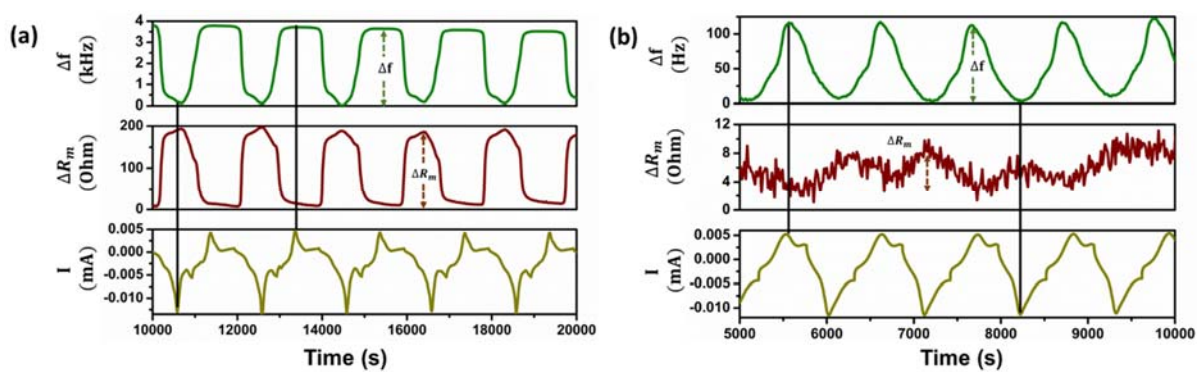


Figure S10: Frequency change (Δf), motional resistance change (ΔR_m) and current variation with time carried out at a scan rate of 1 mV s^{-1} in (a) 1 M ZnSO_4 solution and (b) 0.25 M AlCl_3 solution.

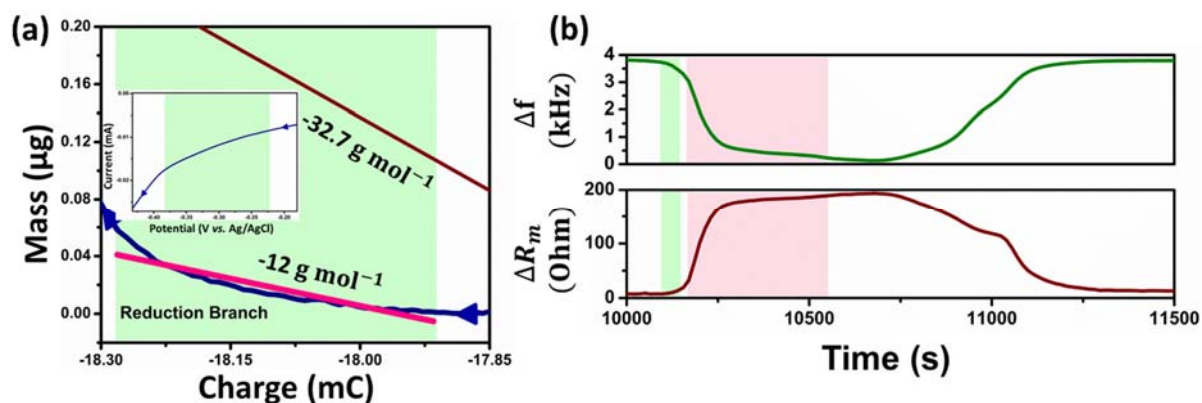
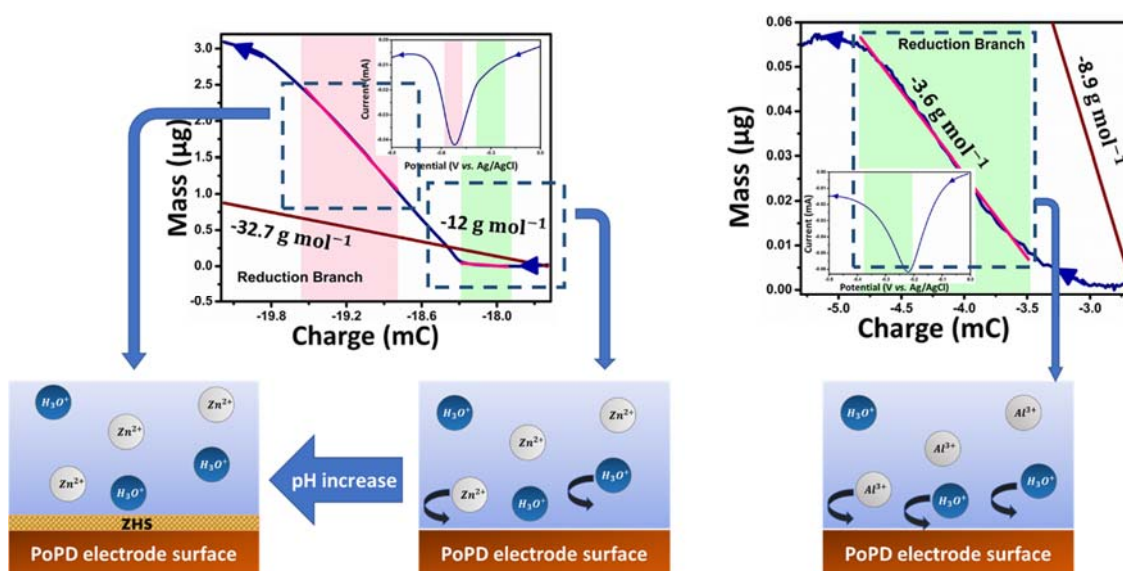


Figure S11: (a) Electrode mass change vs. charge during reduction (Enlarged version from Figure 5a in the main manuscript) in (a) 1 M ZnSO_4 ; (b) Frequency change (Δf) and motional resistance change (ΔR_m) with time (enlarged version from Figure S10a) in 1 M ZnSO_4 solution.



Scheme 1. Schematic description of dissimilar behavior of PoPD in the different electrolytes.

H. EDX spectrum of the cycled PoPD electrodes

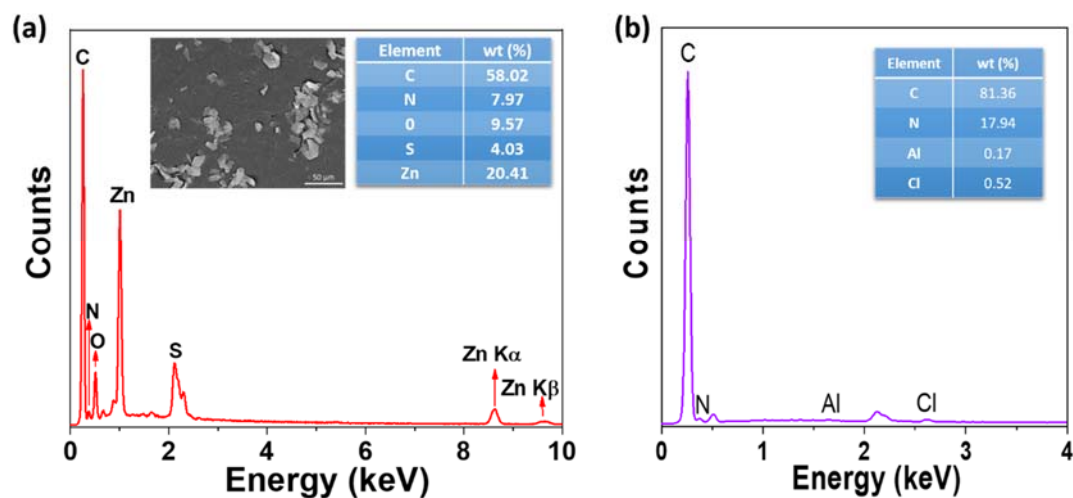


Figure S12: (a) EDS spectrum of PoPD after fully discharged to -0.95 V *vs.* Ag/AgCl (a) in 1 M ZnSO₄, (b) in 0.25 M AlCl₃.

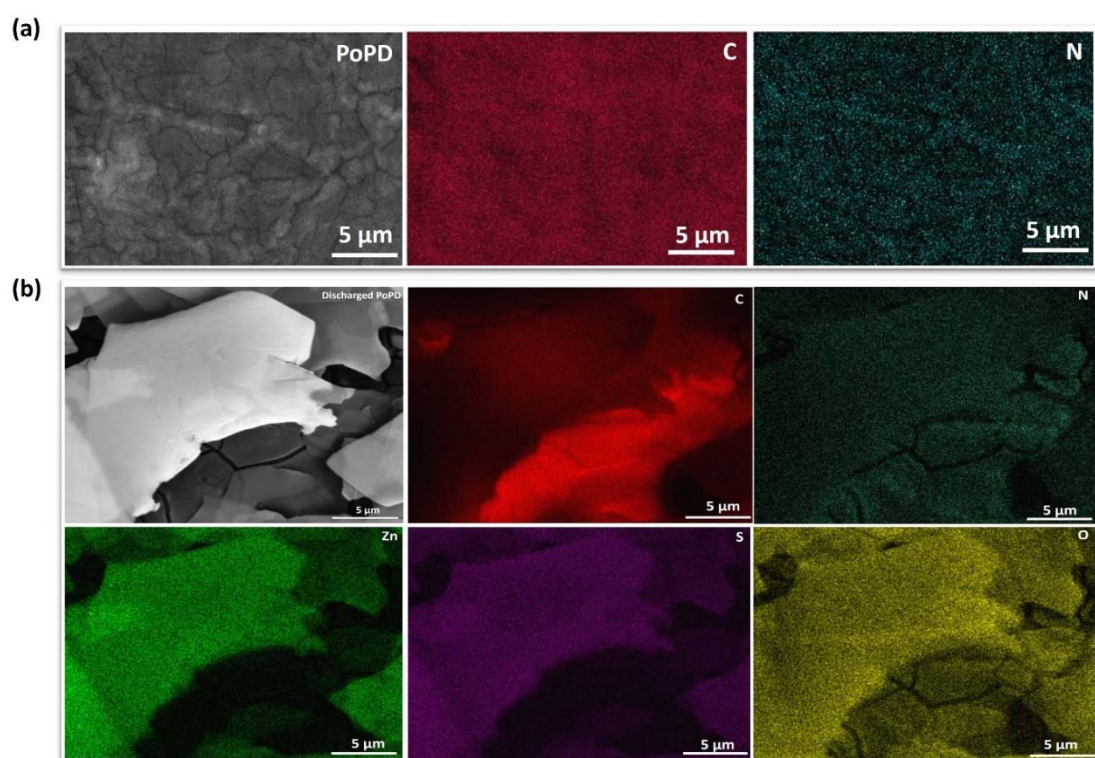
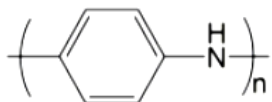
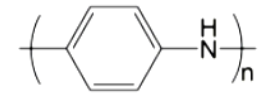
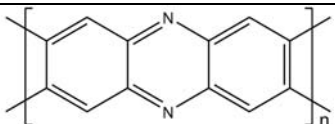
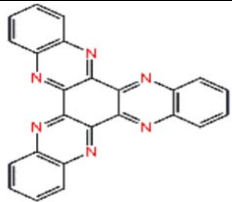
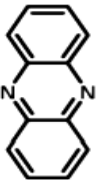


Figure S13. SEM elemental mappings of (a) Pristine PoPD electrode and corresponding elements (C, N), (b) Fully discharged PoPD electrode in 1 M ZnSO₄ and corresponding elements (C, N, Zn, S, O).

Part I. Literature comparisons

Table 1. Organic cathode materials in aqueous electrolyte Zn-ion batteries

Host Structure	Electrolyte	Discharge capacity, capacity retention, current density, cycle number	Reference
 Sulfo self-doped PANI-S	1 M ZnSO ₄	110 mAh g ⁻¹ , 10 A g ⁻¹ , 2000 cycles	[1]
 PANI/CF	1 M Zn(CF ₃ SO ₃) ₂	95 mAh g ⁻¹ , 5 A g ⁻¹ , 3000 cycles	[2]
 PoPD	2 M ZnSO ₄	157 mAh g ⁻¹ , 1 A g ⁻¹ , 3000 cycles	[3]
 diquinoxalino [2,3-a:2',3'-c] phenazine (HATN)	2 M ZnSO ₄	140 mAh g ⁻¹ , 93.3%, 5 A g ⁻¹ , 5000 cycles	[4]
 Phenazine	2 M ZnSO ₄	85 mAh g ⁻¹ , 79%, 1 A g ⁻¹ , 1000 cycles	[5]

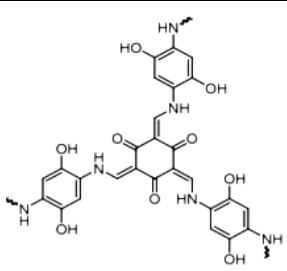


 <p>HqTp</p>	3 M ZnSO ₄	85 mAh g ⁻¹ , 95%, 3.75 A g ⁻¹ , 1000 cycles	[6]
 <p>PoPD (repeating unit)</p>	1 M ZnSO ₄	93 mAh g ⁻¹ , 65 %, 5C, 1000 cycles	This work

Table 2. Organic cathode materials in aqueous electrolyte Al-ion batteries

Host Structure	Electrolyte	Discharge capacity, capacity retention, current density, cycle number	Reference
poly (3,4,9,10-perylentetracarboxylic diimide) (PPTCDI)	0.5 M AlCl ₃	185 mAh g ⁻¹ , 100%, 100 mA g ⁻¹ , 1000 cycles	[7]
macrocyclic calix[4]quinone (C4Q)	1 M Al(OTF) ₃	333 mAh g ⁻¹ , 81%, 200 mA g ⁻¹ , 50 cycles	[8]
Phenazine	5 M Al(OTF) ₃	132 mAh g ⁻¹ , 76.5 %, 50 mA g ⁻¹ , 300 cycles	[9]
9,10-anthraquinone	1 M Al ₂ (SO ₄) ₃	211.4 mAh g ⁻¹ , 94.5 %, 800 mA g ⁻¹ , 500 cycles	[10]
tetrachloro-1,4-benzoquinone (TCQ)	1 M Al(OTF) ₃	100 mAh g ⁻¹ , 71.8 %, 2 A g ⁻¹ , 300 cycles	[11]

 <p>PoPD (repeating unit)</p>	0.25 M AlCl ₃	110 mAh g ⁻¹ , 56%, 5C, 1000 cycles	This work
--	--------------------------	--	-----------

References

- [1] H.Y. Shi, Y.J. Ye, K. Liu, Y. Song, X.Q. Sun, A Long-Cycle-Life Self-Doped Polyaniline Cathode for Rechargeable Aqueous Zinc Batteries, *Angewandte Chemie-International Edition*, 57 (2018) 16359-16363.
- [2] F. Wan, L.L. Zhang, X.Y. Wang, S.S. Bi, Z.Q. Niu, J. Chen, An Aqueous Rechargeable Zinc-Organic Battery with Hybrid Mechanism, *Advanced Functional Materials*, 28 (2018).
- [3] S.Q. Zhang, S.T. Long, H. Li, Q. Xu, A high-capacity organic cathode based on active N atoms for aqueous zinc-ion batteries, *Chemical Engineering Journal*, 400 (2020).
- [4] Z.W. Tie, L.J. Liu, S.Z. Deng, D.B. Zhao, Z.Q. Niu, Proton Insertion Chemistry of a Zinc-Organic Battery, *Angewandte Chemie-International Edition*, 59 (2020) 4920-4924.
- [5] Q. Wang, Y. Liu, P. Chen, Phenazine-based organic cathode for aqueous zinc secondary batteries, *Journal of Power Sources*, 468 (2020).
- [6] M.A. Khayum, M. Ghosh, V. Vijayakumar, A. Halder, M. Nurhuda, S. Kumar, M. Addicoat, S. Kurungot, R. Banerjee, Zinc ion interactions in a two-dimensional covalent organic framework based aqueous zinc ion battery, *Chemical Science*, 10 (2019) 8889-8894.
- [7] R.B. Cang, Y.P. Song, K. Ye, K. Zhu, J. Yan, J.L. Yin, G.L. Wang, D.X. Cao, Preparation of organic poly material as anode in aqueous aluminum-ion battery, *Journal of Electroanalytical Chemistry*, 861 (2020).
- [8] Y.X. Li, L.J. Liu, Y. Lu, R.J. Shi, Y.L. Ma, Z.H. Yan, K. Zhang, J. Chen, High-Energy-Density Quinone-Based Electrodes with Al(OTf) (2+) Storage Mechanism for Rechargeable Aqueous Aluminum Batteries, *Advanced Functional Materials*, 31 (2021).
- [9] J.C. Chen, Q.N. Zhu, L. Jiang, R.Y. Liu, Y. Yang, M.Y. Tang, J.W. Wang, H. Wang, L. Guo, Rechargeable Aqueous Aluminum Organic Batteries, *Angewandte Chemie-International Edition*, 60 (2021) 5794-5799.
- [10] L.J. Yan, C.X. Zhao, Y. Sha, Z.H. Li, T.F. Liu, M. Ling, S.D. Zhou, C.D. Liang, Electrochemical redox behavior of organic quinone compounds in aqueous metal ion electrolytes, *Nano Energy*, 73 (2020).
- [11] J.J. He, X. Shi, C.S. Wang, H.Z. Zhang, X.Q. Liu, Z.J. Yang, X.H. Lu, A quinone electrode with reversible phase conversion for long-life rechargeable aqueous aluminum-metal batteries, *Chemical Communications*, 57 (2021) 6931-6934.